Disruption of the mouse *Jhy* gene causes abnormal ciliary microtubule patterning and juvenile hydrocephalus

Oliver K. Appelbe[1], **Bryan Bollman**[1], **Ali Attarwala**[1], **Lindy A. Triebes**[1], **Hilmarie Muniz-Talavera**[1], **Daniel J. Curry**[2,*], and **Jennifer V. Schmidt**[1]

[1]Department of Biological Sciences, University of Illinois at Chicago, Chicago, IL

[2]Department of Neurosurgery, University of Chicago, Chicago, IL

SUMMARY

Congenital hydrocephalus, the accumulation of excess cerebrospinal fluid (CSF) in the ventricles of the brain, affects one of every 1,000 children born today, making it one of the most common human developmental disorders. Genetic causes of hydrocephalus are poorly understood in humans, but animal models suggest a broad genetic program underlying the regulation of CSF balance. In this study, the random integration of a transgene into the mouse genome led to the development of an early onset and rapidly progressive hydrocephalus. *Juvenile hydrocephalus* transgenic mice (Jhy^{lacZ}) inherit communicating hydrocephalus in an autosomal recessive fashion with dilation of the lateral ventricles observed as early as postnatal day 1.5. Ventricular dilation increases in severity over time, becoming fatal at 4-8 weeks of age. The ependymal cilia lining the lateral ventricles are morphologically abnormal and reduced in number in $Jhy^{lacZ/lacZ}$ brains, and ultrastructural analysis revealed disorganization of the expected 9+2 microtubule pattern. Rather, the majority of $Jhy^{lacZ/lacZ}$ cilia develop axonemes with 9+0 or 8+2 microtubule structures. Disruption of an unstudied gene, *4931429I11Rik* (now named *Jhy*) appears to underlie the hydrocephalus of $Jhy^{lacZ/lacZ}$ mice, and the *Jhy* transcript and protein are decreased in $Jhy^{lacZ/lacZ}$ mice. Partial phenotypic rescue was achieved in $Jhy^{lacZ/lacZ}$ mice by the introduction of a bacterial artificial chromosome (BAC) carrying 60-70% of the JHY protein coding sequence. *Jhy* is evolutionarily conserved from humans to basal vertebrates, but the predicted JHY protein lacks identifiable functional domains. Ongoing studies are directed at uncovering the physiological function of JHY and its role in CSF homeostasis.

INTRODUCTION

The cerebral spinal fluid (CSF) within the ventricles of the brain functions to cushion, nourish and cleanse the brain tissues, and acts as a carrier for key growth factors and

Correspondence to: Jennifer V. Schmidt, University of Illinois at Chicago, Department of Biological Sciences (MC 567), 900 South Ashland Avenue, Chicago, IL 60607. jvs@uic.edu.
*Current Address: Department of Neurosurgery, Texas Children's Hospital, Houston, TX.

signaling molecules (Davson and Segal, 1996; Rodriguez, 1976; Wood, 1983). CSF is continually produced by the choroid plexus tissue within the ventricles, and flows from the lateral and third ventricles through the narrow aqueduct of Sylvius into the fourth ventricle (Welch, 1963; Worthington and Cathcart, 1966; Yamadori and Nara, 1979). CSF flow is accomplished by the movement of cilia on the surface of the ependymal cells lining the ventricles, and likely also by pulsatile changes in intracranial blood flow (Bhadelia et al., 1997; Greitz, 1993; Quencer et al., 1990). From the fourth ventricle, the fluid exits the brain, moving into the spinal canal and the subarachnoid space. CSF production is balanced by its removal; once thought to occur only through the arachnoid villi into the bloodstream, it is now believed that both the lymphatic system and the ventricular ependymal cells play a role in CSF uptake (Koh et al., 2006; Oi and Di Rocco, 2006; Weller et al., 1992).

An increase in the amount of CSF within the closed space of the brain results in the disease known as hydrocephalus. Congenital hydrocephalus is one of the most common human developmental disorders, and may present nonsyndromically or in conjunction with a number of developmental malformations. Population-based studies estimate an incidence of 0.4 to 0.8 in 1000 children born with hydrocephalus in the absence of any neural tube defect (Blackburn and Fineman, 1994; Christensen et al., 2003; Schrander-Stumpel and Fryns, 1998; Stoll et al., 1992). Physiologically, hydrocephalus may be caused by 1) overproduction of CSF, 2) failure to resorb CSF, or 3) a blockage that prevents flow through the ventricles. Hydrocephalus is categorized as either communicating, in which there is no physical blockage to CSF flow, or noncommunicating, in which CSF flow is blocked, usually at the aqueduct. As the volume of CSF in the ventricles increases, the pressure on surrounding brain tissues leads to neuronal cell death. Left untreated, progressive tissue destruction leads to physical and cognitive decline and eventual death (Gadsdon et al., 1979).

Congenital hydrocephalus, in which the disease presents at or shortly after birth, is often associated with subarachnoid hemorrhage, where residual blood products are believed to occlude the arachnoid (Rudas et al., 1998). It has been estimated that 60% of the cases of congenital hydrocephalus in human infants are acquired, with an identifiable pathology, while the other 40% have no known cause and are likely genetic in origin (Haverkamp et al., 1999). One known genetic cause of congenital hydrocephalus in humans is mutation of the gene encoding the L1CAM cell adhesion protein, although studies show a strong heritable component to the development of hydrocephalus (Castro-Gago et al., 1996; Chalmers et al., 1999; Chow et al., 1990; Chudley et al., 1997; Hamada et al., 1999; Koh and Boles, 1998; Munch et al., 2012; Portenoy et al., 1984; Rosenthal et al., 1992; Verhagen et al., 1998; Vincent et al., 1994).

The study of animal models has uncovered numerous mechanisms that may underlie the development of hydrocephalus. For example, abnormal differentiation of the arachnoid layer in mice deficient in the forkhead gene *Foxc1* leads to communicating hydrocephalus due to a decrease in CSF absorption (Green, 1970; Kume et al., 1998). Deletion of a genomic segment encompassing the human *FOXC1* gene has been associated with hydrocephalus in four human patients (Kume et al., 1998). Abnormal development of the subcommissural organ, overproduction of CSF by the choroid plexus, ependymal denudation or disorganization, and defects in ependymal cilia have also been shown to cause hydrocephalus in mouse and rat models (Banizs et al., 2005; Batiz et al., 2006; Blackshear et al., 2003; Davy and Robinson, 2003; Feng et al., 2009; Ibanez-Tallon et al., 2004; Jones and Bucknall, 1988; Krebs et al., 2004; Lechtreck et al., 2008; Lindeman et al., 1998; Sapiro et al., 2002; Tullio et al., 2001; Wilson et al., 2010).

Enhancer trapping, the random integration of a minimal promoter-reporter transgene, can localize genes active in specific tissues or at specific times during development (Allen et al., 1988). Insertional mutagenesis during the generation of transgenic mice is common, and enhancer traps may confer such mutations when they not only "trap", but also inactivate, a gene or its regulatory elements. A promoter mapping transgene generated in our laboratory inadvertently functioned as an enhancer trap, conferring widely varying *lacZ* expression patterns across independent transgenic lines. One of these lines showed *lacZ* expression in the embryonic and adult brain, and as homozygotes, the mice developed a rapidly progressing juvenile hydrocephalus. These *Juvenile hydrocephalus* mice (formally *Jhy$^{Tg(Dlk1-lacZ)1Jvs}$*, here abbreviated *Jhy^{lacZ}*) show overt doming of the skull by one week after birth, and die or must be sacrificed by 4-8 weeks of age. Histological analysis shows the open aqueduct indicative of communicating hydrocephalus, and electron microscopy identified altered microtubule organization of the ependymal cilia. Mapping of the transgene integration site found that it disrupted the previously unstudied gene *4931429I11Rik* (now named *Jhy*). The integration and an associated deletion remove a splice acceptor site within the *Jhy* gene, suggesting reduced function of *Jhy* is causative for the phenotype. The *Jhy* gene is conserved across vertebrates, but has no homology to other genes in the mouse genome, and carries no identifiable functional domains. This manuscript provides a detailed description of the *Jhy$^{lacZ/lacZ}$* mouse phenotype; characterization of the *Jhy* gene is ongoing.

METHODS

Jhy^{lacZ} mice

The *Juvenile hydrocephalus* transgene (*Jhy^{lacZ}*) was generated from the promoterless *lacZ* vector pNASS- (Clontech, Mountain View, CA). A genomic fragment from −248 bp to +50 bp relative to the *Dlk1* transcriptional initiation site (Osoegawa et al., 2000) was isolated and cloned into the vector. The transgene (-*248Dlk1lacZ*), including the *Dlk1* promoter, SV40 splice donor-acceptor site, *lacZ* gene, and polyadenylation signal, was then excised, gel purified, and injected into FVB/N fertilized mouse eggs with the assistance of the University of Illinois at Chicago Transgenic Production Service. Offspring were genotyped by PCR using primers spanning the junction between the *Dlk1* promoter (OL410, 5 -GGGGACGACAGTACGAAAAGGC-3) and the *lacZ* gene (OL411, 5 -GTATCGGCCTCAGGAAGATCGC-3). DNA for genotyping was obtained from tail clips, digested by proteinase K overnight, phenol:chloroform extracted, and ethanol precipitated. Twelve transgenic lines were established on an FVB/N background and analyzed for *lacZ* expression. The *Jhy^{lacZ}* line is maintained by intercrossing *Jhy$^{lacZ/+}$* animals. *Jhy^{lacZ}* mice were genotyped using two sets of primers that amplified either the wild type allele (OL1408, 5 -AAGCTCTGTCTGGGCTCACAATCT-3 ; OL1409, 5 -TGACCTCTTGGGACATTGCCTGAT-3) or the *Jhy^{lacZ}* allele (OL1420, 5 -TCCAGTTCAACATCAGCCGCTACA-3 ; OL1395, 5 -TTAGAAGCGTTCGTTTGTGCAGCC-3). PCR was performed in an Eppendorf Mastercycler (Hauppauge, NY) as follows: 95°C for 5 min; 35 cycles of 94°C for 30 sec, 62°C for 30 sec, and 72°C for 1 min; and a final step of 72°C for 10 min.

β-galactosidase assay for *lacZ* expression

Brains were dissected at postnatal day 0.5 (P0.5) and P5, testes were dissected from adult mice, and both were immediately fixed in 4% paraformaldehyde in 1× PBS for 1 hour on ice. Following fixation, tissues were washed in wash buffer (2 mM $MgCl_2$, 0.01% deoxycholic acid, 0.02% NP-40, in PBS) three times for 30 minutes each at room temperature (RT). Expression of *lacZ* was detected as -galactosidase staining using the detection solution (1 mg/ml ×-gal in DMF, 5 mM potassium ferricyanide, 5 mM potassium ferrocyanide, 2 mM $MgCl_2$, 0.01% deoxycholic acid, 0.02% NP-40, in PBS), incubating

overnight in the dark at RT. The next day, tissues werewashed three times in 1× PBS, dehydrated in solutions of increasing ethanol concentration, and infused with paraffin wax using a Shandon Citadel 1000 tissue processor (Fisher Scientific, Pittsburgh, PA, USA). Processed tissues were embedded in blocks of paraffin using a Shandon Histocentre 2 embedding machine (Fisher Scientific, Pittsburgh, PA). Embedded tissues were cut into 10 μm sections using a microtome (Leica Microsystems RM2125, Bannockburn, IL, USA) and background stained with 10% eosin for 1 minute. Coverslips were applied using Permount (Fisher Scientific, Pittsburgh, PA) and images were taken on a Leica MZFLIII dissecting microscope (Wetzlar, Germany).

Magnetic resonance imaging

MRI was performed at the University of Chicago Magnetic Resonance Imaging & Spectroscopy Research Laboratory. $Jhy^{+/+}$ and $Jhy^{lacZ/lacZ}$ mice at P6 and P13 were sacrificed by CO_2 inhalation approximately one hour prior to imaging. Imaging was performed using a Bruker scanner equipped with a 4.7T magnet and a custom-made birdcage coil for juvenile mice. Coronal T2-weighted axial spin echo images were collected using the parameters: repetition time 3000 ms, echo time 60 ms, array size 256×256, field of view 2.0 cm.

Genomic localization and sequence analysis

The BD GenomeWalker Universal Kit (Clontech, Mountain View, CA) was used to map the integration site of the Jhy^{lacZ} transgene. The GenomeWalker protocol was followed with the following specifications. A library created from DraI digestion of genomic tail DNA was used for mapping the distal transgene integration boundary. Following the purification of digested DNA and ligation of adaptors, nested PCR was performed with the following primers: outer (OL834, 5 -CCCGTTTTTCCCGATTTGGCTACATGACA-3 ; AP1, 5 -GTAATACGACTCACTATAGGGC-3) and inner (OL836, 5 -CAACCGCTGTTTGGTCTGCTTTCTGACAA-3 ; AP2, 5 -ACTATAGGGCACGCGTGGT-3). The proximal boundary of the transgene integration was mapped using the following primers: OL1368, 5 -AACACTTTCATGGATCCTGAGGACA-3 ; OL1618, 5 -GTAACCGTGCATCTGCCAGTTTG-3 . PCR products were sequenced by the University of Illinois at Chicago Research Resources Center DNA Services facility (Chicago, IL). Cross-species Jhy cDNA and protein alignments were performed in Geneious v5.6.6 (Biomatters Ltd) using Geneious and ClustalW alignments, respectively, with the default parameters.

Quantitative RT-PCR

Total RNA was extracted from P0.5 mouse brains using LiCl-urea precipitation (Auffray and Rougeon, 1980), and DNA contamination was removed using TURBO DNA-*free* (Ambion, Austin, TX). Reverse transcription was performed with 1 μg of total RNA using Superscript III reverse transcriptase (Invitrogen, Carlsbad, CA). The cDNA was diluted 1:10, and 2 μl was used for PCR analysis. Control reactions were performed without reverse transcriptase. Quantitative RT-PCR (qRT-PCR) was performed using the DNA Engine Opticon 2 (MJ Research, Hercules, CA) with the following primers: Jhy, OL1366, 5 -AGCCAACAACACTAACAGGGAAGA-3 and OL1524, 5 -TCCAGTTGGGGATCATATCGGAGGT-3 that span exons 2-3; Bsx, OL1325, 5 -CAGAACCGGCGGATGAAGCATAAA-3 and OL1326, 5 -ACTTCGTCCTCGGGCTCAGTAA that lie within exon 3; $Crtam$, OL1114, 5 -AGCACACGTGGTATGGAAGAAGGA and OL1115, 5 -TTTGGCTCCCGAGTATAACTGCGT that span exons 8-10; -actin, OL1112, 5 -TCTTGGGTATGGAATCCTGTGGCA-3 and OL1113, 5 -

TCTCCTTCTGCATCCTGTCAGCAA-3 . For all primer pairs qRT-PCR was performed using SYBR GreenER (Invitrogen, Carlsbad, CA) under the following conditions: 50°C for 2 min; 95°C for 10 min; followed by 40 cycles of 94°C for 15 sec, 62°C for 30 sec, 72°C for 15 sec. A melting curve ranging from 60°C to 95°C was run after each reaction to test for primer dimerization or the formation of multiple products.

Tg^{BAC} rescue mice

The BAC clone RP23-273J15 was obtained from the Children's Hospital Oakland Research Institute (Oakland, CA). BAC DNA was linearized with *Bsp*EI and prepared for injection by phenol:chloroform extraction, ethanol precipitation, and resuspension in microinjection buffer (10 mM Tris-HCl pH 7.5, 0.1 mM EDTA, 30 μM spermine, 70 μM spermidine, 100 mM NaCl). The linearized BAC was microinjected into FVB/N fertilized mouse eggs with the assistance of the University of Illinois at Chicago Transgenic Production Service and 38 offspring were produced. Pups were genotyped for the BAC from tail DNA using the primer set: OL1183, 5 -CGACTCAAGCCTTCGCGAAAGAAA-3 ; OL1561, 5 - CGTGTTTGAAGTGATCAGCGGCTT-3 . Five of the 38 transgenic mice were positive for the BAC, and one expressing transgenic line was generated on the FVB/N background. Formally *Tg(RP23-273J15)1Jvs*, this line is here abbreviated Tg^{BAC}.

Scanning electron microscopy

Jhy^{+/+}, Jhy^{lacZ/+}, and *Jhy^{lacZ/lacZ}* littermate P5 brains were dissected and fixed in Karnovsky's fixative (2.5% glutaraldehyde, 2.0% paraformaldehyde, 0.1 M sodium cacodylate buffer pH 7.4) for 4 days at RT. Dissecting the left and right hemispheres away from the midbrain and removing the hippocampus exposed the lateral ventricles. Brains were washed 3 times in PBS at RT, then dehydrated in a graded ethanol series on ice with the 100% ethanol solution containing molecular sieves. The preparations were dried in a Bal-Tec CPD 030 Critical Point Dryer (Bal-Tec AG, Fürstentum, Liechtenstein), coated with gold/palladium using a DentonVacuum Desk IV Sputter Coater (Denton Vacuum LLC, Moorestown, NJ) set at 48% power, and imaged directly on a JEOL 5600 LV scanning electron microscope (JEOL, Peabody, MA). The accelerating voltage was set at 15 kV, with the higher magnification images taken at 20 kV.

Transmission electron microscopy

Jhy^{+/+} and *Jhy^{lacZ/lacZ}* brains were dissected at P5 and immersed in Karnovsky's fixative for seven days. The lateral ventricles were isolated and further fixed in Karnovsky's for an additional 24 hours. The tissue was washed in three changes of 0.1 M sodium cacodylate buffer pH 7.4 and immersed in 1% osmium tetroxide in 0.1 M sodium cacodylate buffer pH 7.4 for two hours at RT. The tissue was again washed in 0.1 M sodium cacodylate buffer pH 7.4 and then dehydrated using increasing concentrations of ethanol. The tissue was infiltrated overnight with 1 part 100% ethanol and 1 part Spurr's resin, and two additional changes with pure Spurr's resin were made over a 24-hour period. Finally, the tissue was embedded with Spurr's resin in Eppendorf tubes, and polymerized at 70°C for 48 hours. The polymerized blocks were trimmed and faced off at 1 μm sections using a Reichert-Jung Ultracut E Ultramicrotome (Leica Microsystems, Buffalo Grove, IL). The 1 μm sections were placed on glass slides, dyed with 1% toluidine blue, and viewed to determine the region to be used for imaging. Next, 80 nm sections were cut and picked up onto 200 hex mesh nickel parlodion carbon coated grids and allowed to completely dry. The sections were stained for 5 minutes in lead citrate, followed by three washes in deionized water. Once dried, the sections were stained for 45 minutes with uranyl acetate (4% aqueous), followed by three washes in deionized water. The sections were dried, and stained for an additional 5 minutes with lead citrate, followed by three washes in deionized water, and allowed to

completely dry. The sections were viewed using a JEOL 1200EX transmission electron microscope (JEOL, Peabody, MA, USA), and areas of interest were photographed.

Statistical analysis

Two-tailed Student's t-tests were used to calculate the significance of data obtained in qRT-PCR experiments. Standard error of the mean was used to calculate error bars.

Immunofluorescence

P5 mouse brains were fixed in Bouin's fixative for 18-24 hours at RT, then cleared and stored in 70% ethanol. Tissues were then dehydrated, embedded in paraffin and sectioned with a microtome to 8 μm. Standard immunofluorescence techniques were used, with variations as follows. For JHY detection, sections were dewaxed with xylene and rehydrated through a series of ethanol washes. Heat induced antigen retrieval (0.3% Sodium Citrate, 0.05% Tween-20 pH 6.0) was performed followed by washing in PBS. Slides were blocked using 5% donkey normal serum, 1% BSA, 0.5% Tween-20, 0.75% glycine in PBS for 1 hour at RT, and incubated at 4°C overnight with primary antibody against JHY (1:10; Sigma-Aldrich, HPA039612). The sections were then incubated with Alexa Fluor 647-conjugated secondary antibody for 2 hours at RT (1:250; Jackson ImmunoResearch Laboratories, West Grove, PA). Finally, the slides were DAPI stained (D1306; Life Technologies, Grand Island, NY.) and mounted using Vectashield mounting medium (H1000; Vector Laboratories, Burlingame, CA).

RESULTS

Enhancer trapping identifies a gene required for CSF balance

An experiment was designed to identify regulatory elements of the mouse *Delta-like 1* (*Dlk1*) gene (Fay et al., 1988; Laborda et al., 1993; Okamoto et al., 1997; Smas and Sul, 1993). Varying lengths of the *Dlk1* upstream region were linked to a *lacZ* reporter gene and injected into fertilized FVB/N mouse eggs, generating 12 independent transgenic lines. When analyzed for *lacZ* expression during midgestation, embryos from the different lines showed widely varying patterns of expression, none of them resembling the well characterized pattern of *Dlk1* (data not shown). Enhancer trapping can occur unintentionally, when a transgene that is believed to carry an enhancer either has no enhancer, or it is overwhelmed by stronger regulatory elements at the site of integration. Analysis of the *Dlk1* upstream region subsequently found that no developmental enhancers lie within the transgene sequences; the *Dlk1-lacZ* transgenes functioned instead as enhancer traps (Rogers et al., 2012; Yevtodiyenko et al., 2004).

One transgenic line, examined as whole mount embryos at embryonic day 11.5 (e11.5), showed *lacZ* expression in a small region on the dorsal aspect of the head (Fig. 1A-C). Histologic analysis identified the expressing structure as the epiphysis, the roof of the diencephalon that will form the pineal gland (Fig. 1C). Intercrossing the transgenic animals showed that mice homozygous for the transgene develop progressive and ultimately fatal juvenile hydrocephalus (Fig. 1D, E). None of the other transgenic lines exhibited any degree of hydrocephalus, suggesting the phenotype results from an insertional mutation generated by the transgene, rather than expression of the transgene itself. The transgene integration therefore trapped, and likely altered the function of, a gene required for proper CSF balance in the developing mouse brain. The transgenic mouse line has therefore been named *Jhy^{lacZ}* for *Juvenile hydrocephalus*.

Jhy^{lacZ/lacZ} mice show early and progressive hydrocephalus

Heterozygous *Jhy^{lacZ/+}* mice appear normal in all aspects, and showed no evidence of hydrocephalus. Intercrossing *Jhy^{lacZ/+}* animals gave offspring that appeared normal at birth, and all genotypes were found in the expected ratios. As the *Jhy^{lacZ/lacZ}* homozygous mice grew, however, 63% began to display the domed head indicative of hydrocephalus between 2 and 5 weeks after birth (Fig. 1D, E; Fig. 2A). The enlargement of the head progresses rapidly, and as the disease worsens the mice become ataxic and begin to lose weight, likely from motor deficits that interfere with feeding (Fig. 1D). Intracranial hemorrhaging can often be observed externally in the albino FVB/N mice, though this occurs relatively late in the course of the disease and appears to be secondary to the hydrocephalus (Fig. 1E). Histological analysis of the brains of *Jhy^{lacZ/lacZ}* animals at P5 shows dramatically enlarged lateral ventricles and loss of neuronal tissue (Fig. 1F, G). All of these early onset hydrocephalic mice have died, or been sacrificed for humane reasons, by 4-8 weeks of age (Fig. 2B). A small percentage of *Jhy^{lacZ/lacZ}* mice do not show the skull doming of early hydrocephalus, but begin to display the related ataxia and weight loss at 5-6 weeks of age (Fig. 2C). The lack of a skull phenotype is expected in these late onset animals, as the fusion of the anterior frontal cranial suture between 3 and 6 weeks of age prevents skull enlargement beyond this point (Bradley et al., 1996). These late onset mice were followed until 12 weeks of age and all survived to this time point, suggesting a milder course of the disease. Overall, 74% of *Jhy^{lacZ/lacZ}* mice develop hydrocephalus, the majority as juveniles.

Jhy^{lacZ/lacZ} mice show normal brain patterning

Juvenile hydrocephalus can be secondary to abnormal brain development or patternin g, when malformations may physically obstruct CSF flow (Partington, 2001; Pattisapu, 2001). Developmental malformation syndromes are characterized by gross defects in brain structure, or by more subtle disorganization of the cortical layers. To more closely analyze the neuronal development of *Jhy^{lacZ/lacZ}* mice, brains were examined by histological analysis at e18.5, P0.5 and P5. *Jhy^{lacZ/lacZ}* brains appear structurally normal at e18.5 with normal ventricular size and shape and open communication between the ventricles (data not shown). Serial sectioning was then performed through entire *Jhy^{+/+}* and *Jhy^{lacZ/lacZ}* mouse brains at P0.5, prior to the onset of hydrocephalus (Fig. 3A-H). No changes were seen in comparison to *Jhy^{+/+}* littermates, and all existing brain structures appeared correctly patterned. By P1.5 mild hydrocephalus is evident in many *Jhy^{lacZ/lacZ}* brains (data not shown), and at P5 the lateral and third ventricles of *Jhy^{lacZ/lacZ}* mice are significantly larger than their *Jhy^{+/+}* littermates (Fig. 1F, G). The aqueduct and fourth ventricle do not appear enlarged at any stage observed, and the aqueduct remains patent at P0.5, as visualized in transverse and coronal sections (Fig. 3I and data not shown). These data indicate that *Jhy^{lacZ}* mice suffer from communicating hydrocephalus, in the absence of any developmental malformation.

To examine the progression of the disease in the intact animal, magnetic resonance imaging (MRI) was used to view the brains of *Jhy^{+/+}* and *Jhy^{lacZ/lacZ}* littermates (Fig. 3J-M). At P6, dilation of the lateral ventricles can be seen in *Jhy^{lacZ/lacZ}* brains as compared to age matched *Jhy^{+/+}* brains (Fig. 3J, K). At P13, the ventricular dilation in *Jhy^{lacZ}* brains has increased, with a corresponding loss of brain tissue and thinning of the overlying cortex (Fig. 3L, M). The dorsal region of the third ventricle is noticeably dilated at P13 (data not shown); the ventral region of the third ventricle and the fourth ventricle were not visualized in this analysis.

Jhy^{lacZ/lacZ} hydrocephalus is nonsyndromic

Hydrocephalus, in both mouse models and human patients, may occur as one component of certain generalized ciliopathies (Baker and Beales, 2009; Lee, 2011). Individuals suffering

from these ciliary dysfunction syndromes display other cilia-related phenotypes that include situs inversus, infertility and recurrent respiratory infections (Ferkol and Leigh, 2012). No *Jhy^{lacZ/lacZ}* mice were found to display situs inversus, and they showed no evidence of respiratory infections during several years of maintenance. Histological analysis was performed on all major organ systems of *Jhy^{+/+}* and early onset *Jhy^{lacZ/lacZ}* mice at 4 weeks of age (Fig. 3N-Q and data not shown). Particular attention was paid to those tissues involved in ciliary-related disease syndromes, such as the lungs, kidney and testis. With the exception of the testes, no alterations were found in any of the tissues examined. Overall testis structure was normal in *Jhy^{lacZ/lacZ}* mice, but there appeared to be reduced numbers of mature, flagellated sperm in the lumen of many tubules (Fig. 3N, O). As one example of an unaffected tissue, the structure of the kidney was unaltered in *Jhy^{lacZ/lacZ}* mice as compared to *Jhy^{+/+}* (Fig. 3P, Q). The effects of the *Jhy^{lacZ}* mutation are therefore limited to the brain and the testes.

Fertility can be difficult to analyze in early lethal mutations, and most early onset *Jhy^{lacZ/lacZ}* mice are quite debilitated by breeding age. No early onset *Jhy^{lacZ/lacZ}* mice have produced pregnancies, but two of the late onset animals have given offspring. The longest surviving hydrocephalic *Jhy^{lacZ/lacZ}* mouse, a male, fathered a litter of 4 pups with an FVB/N female at 2 months of age. One female *Jhy^{lacZ/lacZ}* animal gave birth to a litter of 6 pups at 3 months of age when crossed to a *Jhy^{lacZ/+}* male. The *Jhy^{lacZ/lacZ}* offspring of this *Jhy^{lacZ/lacZ}* female showed no phenotypic differences from *Jhy^{lacZ/lacZ}* pups of a *Jhy^{lacZ/+}* female. *Jhy^{lacZ/lacZ}* mice are therefore fertile, but males may show subfertility due to reduced sperm numbers, and most animals of both sexes do not breed due to the rapid progression of the hydrocephalus phenotype.

The Jhy^{lacZ} reporter is expressed in the brain

The expression pattern of an enhancer trap transgene integrated into the mo use genome typically reflects that of a gene or genes near the integration site. The integration of the *Jhy^{lacZ}* transgene within the *Jhy* gene suggests that *lacZ* may serve as a proxy for the expression of *Jhy* and/or other genes in the region. To further characterize the transgene expression pattern, *lacZ* expression was analyzed at P0.5 and P5. At P0.5, *lacZ* expression is visible in the pineal gland (Fig. 4A, B, E, F), in the hypothalamus (Fig. 4A, B, M, N), and in the ependymal cells of the aqueduct of Sylvius (Fig. 4Q, R). At P5, expression is similarly observed in the pineal (Fig. 4C, D, G, H), the hypothalamus (Fig. 4C, D, O, P) and the ependyma of the aqueduct of Sylvius (Fig. 4S, T). At this stage expression is also seen in the choroid plexus of the third ventricle but not the choroid plexus of the lateral or fourth ventricles (Fig. 4K, L). Expression of the *lacZ* reporter within the developing brain is consistent with a causative role for the transgene integration in the hydrocephalus of *Jhy^{lacZ/lacZ}* mice. The choroid plexus and ependymal cells both play key roles in CSF balance, with the choroid responsible for producing the bulk of the CSF, while ependymal cilia regulate CSF flow and maintain a patent aqueduct (Bruni, 1998).

Ependymal cilia are morphologically abnormal in *Jhy^{lacZ/lacZ}* mice

The motile cilia of the ependymal cells lining the ventricular surfaces play a role in maintaining proper CSF flow through the ventricular system. Defects in ciliary structure or function underlie several mouse models of hydrocephalus as well as certain human cases (al-Shroof et al., 2001; Batiz et al., 2006; Davy and Robinson, 2003; Feng et al., 2009; Ibanez-Tallon et al., 2004; Sapiro et al., 2002; Tullio et al., 2001; Wessels et al., 2003). Scanning electron microscopy (SEM) was used to inspect the developing cilia of P5 *Jhy^{lacZ/lacZ}* mice and their *Jhy^{+/+}* littermates. The P5 time point was chosen with the goal of observing any ciliary changes that may be causative for the hydrocephalus, while avoiding the effects of morphological damage and neuronal loss found at later stages. Opening the ventricles of

Jhy$^{+/+}$ animals invariably caused breakage at the attachment point that joins the ventricular walls (Fig. 5A, arrow). Early ventricular enlargement in *Jhy$^{lacZ/lacZ}$* brains prior to attachment leads to a loss of this adhesion point (Fig. 5B). Ependymal cilia develop along the lateral ventricular walls beginning at birth in a caudorostral-ventrodorsal direction. In *Jhy$^{+/+}$* animals, large portions of the caudal ventricular walls are covered with ciliary tufts, while the cilia are less dense across more rostral areas (Fig. 5A). The cilia display a consistent directional orientation suggestive of the coordinated motion required for laminar flow (Fig. 5C, E). In P5 *Jhy$^{lacZ/lacZ}$* animals, cilia development has progressed equally far across the lateral ventricular wall, but at low magnification the cilia appear less dense than in comparable ventricular regions of *Jhy$^{+/+}$* animals (Fig. 5B, D). A t hig her magnification, the cilia of *Jhy$^{lacZ/lacZ}$* animals are sparser, shorter and of irregular length, and oriented in random directions, suggesting a loss of coordinated movement (Fig. 5F). Similar data were obtained from all regions analyzed across the ciliated areas of the ventricles, regardless of the density of the developing cilia at each region.

Transmission electron microscopy (TEM) was used to analyze the ultrastructure of *Jhy$^{lacZ/lacZ}$* lateral ventricular ependymal cilia in P5 brains. Normal motile cilia display a 9+2 arrangement of microtubule doublets, and this pattern was observed in 99% of the *Jhy$^{+/+}$* ependymal cilia (Fig. 5G and Fig. 8D). In *Jhy$^{lacZ/lacZ}$* mice, only 7% of cilia displayed the normal 9+2 pattern, with 71% of cilia having a 9+0 microtubule arrangement, and 19% having an 8+2 pattern (Fig. 5H, I and Fig. 8D). The microtubule pairs found in the center of *Jhy$^{lacZ/lacZ}$* 8+2 cilia do not display the characteristic singlet morphology of the central pair of normal 9+2 cilia. Rather, they show the asymmetric A/B structure of a peripheral doublet that has moved to the center (Fig. 5I). In some axonemes this aberrant doublet is found positioned between the center of the axoneme and an open position in the outer ring (Fig. 5J). Although further investigation is needed, this pattern suggests a 9+0 ciliary axoneme in the process of reorganizing to form an 8+2 axoneme. All other axonemal components visualized, including the dynein arms and radial spokes, appeared normal (Fig. 5H, I).

The *Jhy^{lacZ}* transgene integrated into an uncharacterized gene, *4931429I11Rik*

Enhancer trapping with a reporter gene allows the bacterially-derived *lacZ* gene to be used as a tag to identify the transgene integration site. The GenomeWalker Universal Kit was used to identify the integration site of the *Jhy^{lacZ}* transgene. An adaptor-tagged restriction library was generated from *Jhy$^{lacZ/lacZ}$* genomic DNA, which served as a template for PCR using primers within the transgene against primers corresponding to the adaptors. Amplification yielded a junction fragment containing the 5 end of the *Jhy^{lacZ}* transgene, along with endogenous flanking sequence that placed the integration on mouse chromosome 9 at 40.9 Mb, within exon 5 of the uncharacterized gene *4931429I11Rik* (Fig. 6A, B). No function has been reported for this gene, and therefore the name *Jhy* has been approved by the Mouse Nomenclature Committee to reflect its presumed role in the *Jhy$^{lacZ/lacZ}$* phenotype. The *Jhy^{lacZ}* transgene integrated at the beginning of *Jhy* exon 5, in the same orientation as the gene (Fig. 6B). To characterize the integration boundary of the 3 end of the transgene, a series of primers were designed within the *Jhy* gene flanking the integration site. Detailed PCR analysis determined that the integration generated a 513 bp deletion that removes 425 bp of intronic sequence plus the exon 5 splice acceptor site and the first 88 bp of *Jhy* exon 5 (Fig. 6B, C).

The *Jhy* gene is conserved across most vertebrate species, with all species analyzed carrying conserved syntenic regions also encompassing *Bsx* and *Crtam*. At the nucleotide level, the mouse *Jhy* cDNA has 72% identity to the human cDNA, 56% to the chicken, and 52% to the zebrafish. In the mouse, *Jhy* has 9 exons that would generate an mRNA of 3068 nucleotides, and encode a protein of 770 amino acids with a molecular weight of 87 kDa. At the protein

level, conservation between mouse and human is 66%, between mouse and chicken 27%, and between mouse and zebrafish 24% (Supplementary Fig. 1). Analysis of the predicted JHY protein revealed no known functional domains, and beyond the single ortholog in all vertebrates there are no obvious paralogs in any species. The biological role of *Jhy* is therefore still to be determined.

Jhy mRNA and protein are reduced in *Jhy^{lacZ/lacZ}* mice

The autosomal recessive inheritance pattern of the *Jhy^{lacZ/lacZ}* phenotype suggests that the integration generated a loss of function or hypomorphic allele of *Jhy*. Quantitative RT-PCR (qRT-PCR) was used to analyze *Jhy* expression levels in the brains of *Jhy^{+/+}*, *Jhy^{lacZ/+}* and *Jhy^{lacZ/lacZ}* mice at P0.5. *Jhy* expression levels were reduced to 85% of wild type in *Jhy^{lacZ/+}* brains and to 41% in *Jhy^{lacZ/lacZ}* brains (Fig. 6D). The primers used for this analysis span *Jhy* exons 2-3, detecting all transcripts containing the 5 end of the *Jhy* gene. The transcriptional termination signal of the *Jhy^{lacZ}* transgene is expected to disrupt all transcripts at the exon 5 integration point, but the actual transcripts produced from this allele are currently unknown. Should transcription proceed beyond the transgene integration site, the deletion of the first 88bp of exon 5 means that a fully wild type transcript cannot be produced.

The *Brain specific homeobox* (*Bsx*) and *Cytotoxic and regulatory T cell molecule* (*Crtam*) genes are closely linked to *Jhy*, with *Bsx* located 17 kb proximal and *Crtam* located 9 kb distal (Fig. 6A). Transgene integrations can cause regional changes in gene expression, and therefore expression of *Bsx* and *Crtam* were similarly examined by qRT-PCR in P0.5 brains. Levels of *Crtam* were not significantly altered in *Jhy^{lacZ/+}* or *Jhy^{lacz/lacZ}* brains, but *Bsx* levels were reduced to 77% of wild type in *Jhy^{lacZ/+}* and to 67% in *Jhy^{lacz/lacZ}* (Fig. 6D). These data suggest a long-range effect of the *Jhy^{lacZ}* transgene, and potential functional linkage of *Jhy* and *Bsx* expression.

To explore the levels of JHY protein in *Jhy^{lacZ}* mice, a commercial antibody generated against the human JHY homolog (C11ORF63) was used (Sigma-Aldrich, St. Louis, MO) (Ivliev et al., 2012). Ivliev, et al carried out a bioinformatics screen for proteins potentially expressed in ciliated cells, identifying C11ORF63 among 74 novel predicted ciliary proteins (Ivliev et al., 2012). Ciliary expression of these proteins was verified with data from the Human Protein Atlas, a high-throughput analysis of protein expression data across human tissues (Uhlen et al., 2010). This study had explored C11ORF63 expression in seve ral ciliated tissues using a peptide antibody directed against the exon 3-encoded region of the predicted C11ORF63 protein. This antibody was obtained and tested against P5 mouse brain, and found to recognize the mouse JHY protein as well (Fig. 7A). This was not surprising, as the C11ORF63 peptide antigen bears 87% identity to the homologous mouse sequence. In *Jhy^{+/+}* P5 mouse brain sections, expression of JHY was seen in the ependymal cells lining the lateral ventricles (Fig. 7A), and scattered cells within deeper layers, but this protein signal was significantly reduced in *Jhy^{lacz/lacZ}* animals (Fig. 7B).

The *Jhy^{lacZ}* phenotype can be rescued by a *Jhy* transgene

The most definitive way to verify that a specific gene underlies a particular phenotype is to cure the phenotype by restoring the candidate gene. Bacterial artificial chromosomes (BACs) are ideal for transgenic rescue, since their large size makes it possible to isolate a gene and its regulatory elements on a single clone. Rescue of the *Jhy^{lacZ}* phenotype was performed using the BAC clone RP23-273J15 that spans the region from 105 kb proximal to 65 kb distal to the *Jhy^{lacZ}* integration site (Fig. 8A) (http://bacpac.chori.org). The RPCI-2 3 library is derived from the C57BL/6 mouse strain, allowing the use of strain-specific polymorphisms to distinguish the endogenous *Jhy* gene from the BAC *Jhy* gene, and

endogenous from BAC-derived transcripts. The BAC clone was linearized and microinjected into FVB/N embryos and a single transgenic mouse line was obtained that both transmitted and expressed the BAC Jhy gene. Formally named $Tg(RP23-273J15)1Jvs$, this line is abbreviated here as Tg^{BAC}. The transgene was crossed into the Jhy^{lacZ} line to generate animals heterozygous for Tg^{BAC} and homozygous for Jhy^{lacZ} ($Tg^{BAC/+};Jhy^{lacZ/lacZ}$).

Analysis of these mice revealed that a single copy of Tg^{BAC} yielded a 50% rescue of $Jhy^{lacZ/lacZ}$ mice, with the incidence of hydrocephalus reduced from 74% in $Jhy^{lacZ/lacZ}$ mice to 37% in $Tg^{BAC/+};Jhy^{lacZ/lacZ}$ mice (Fig. 8B). Phenotypically, $Tg^{BAC/+};Jhy^{lacZ/lacZ}$ animals displayed reduced doming of the skull, though subtle changes were still observed in some animals (Fig. 8C). Further analysis of the Tg^{BAC} integration, however, revealed that the BAC transgene had been truncated within the Jhy gene, likely during integration into the genome. Direct sequencing of PCR products across regions containing single nucleotide polymorphisms between FVB/N (Jhy^{lacZ} background) and C57BL/6 (Tg^{BAC} background) strains were used to determine that Tg^{BAC} was truncated at a position between 419 bp into Jhy exon 5 and 2,420 bp into Jhy intron 5 (Fig. 8A). Interestingly, this point is just slightly 3′ to the position of the Jhy^{lacZ} insertion in the endogenous Jhy gene. Between 60 and 70% of the Jhy protein coding sequence remains on Tg^{BAC} (Fig 8A).

Jhy expression in $Tg^{BAC/+};Jhy^{lacZ/lacZ}$ P0.5 brains was assayed by qRT-PCR using the Jhy exon 2-3 primers and was found to average 113% of wild type levels (data not shown). The Tg^{BAC} transgene therefore restores the level of an, albeit truncated, Jhy mRNA. Bsx expression, which is decreased to 77% of wild type in $Jhy^{lacZ/lacZ}$ brains, was unchanged from this level in $Tg^{BAC/+};Jhy^{lacZ/lacZ}$ mice; this is expected since Bsx is not included on the truncated Tg^{BAC} (Fig. 8A). The increase in Jhy transcription conferred by the Tg^{BAC} transgene was sufficient to enact partial rescue of the ciliary phenotype as well; 32% of ependymal cilia displayed the normal 9+2 microtubule configuration in $Tg^{BAC/+};Jhy^{lacZ/lacZ}$ cilia, compared to only 7% of cilia in $Jhy^{lacZ/lacZ}$ (Fig. 8D). These results suggest that Tg^{BAC} produces a truncated JHY protein that retains partial function.

DISCUSSION

Jhy is a new candidate gene for hydrocephalus

A transgenic insertional mutation on mouse chromosome 9 led to the development of juvenile hydrocephalus, and the subsequent discovery of the Jhy gene. None of the known murine hydrocephalus mutations map to this genomic region, indicating that Jhy^{lacZ} is a new model for juvenile hydrocephalus. $Jhy^{lacZ/lacZ}$ mice develop communicating hydrocephalus during early postnatal development, with the earliest cases visible by histology at P1.5 (Fig. 1 and data not shown). Grossly visible doming of the skull is often observed by 2 weeks of age. These early onset hydrocephalus cases have died or must be sacrificed by 4-8 weeks of age (Fig. 2B). The onset and progression of the Jhy^{lacZ} hydrocephalus varies, however, and a small percentage of animals instead develop a late onset, milder form of the disease (Fig. 2C). These mice show symptoms developing at 5-6 weeks of age, and the animals survive beyond a 12 week monitoring period.

The homozygous recessive inheritance pattern of the Jhy^{lacZ} phenotype suggests the disruption of a gene involved in CSF balance, with reduction or loss of function of this gene causative for the phenotype. Genomic analysis identified the locus disrupted by the transgene as carrying the uncharacterized gene $4931429I11Rik$, now named Jhy. The Jhy gene can be located in all well-annotated vertebrate genomes, from zebrafish through humans. The expression pattern of the Jhy^{lacZ} reporter gene suggests activity in the pineal gland, the hypothalamus, the choroid plexus of the third ventricle, and the ependymal cells

within the aqueduct of Sylvius. The ependymal cells and choroid plexus in particular play key roles in the production and flow of CSF, suggesting altered expression in these tissues might underlie the $Jhy^{lacZ/lacZ}$ phenotype. While these experiments did not detect $lacZ$ expression in the ependyma of the lateral ventricles, preliminary analysis of JHY protein by immunofluorescence indicates that JHY is present in these cells (Fig. 4, Fig. 7).

Ciliary defects in $Jhy^{lacZ/lacZ}$ hydrocephalus

The most striking aspect of the $Jhy^{lacZ/lacZ}$ phenotype is the disorganization and altered morphology of the ependymal cilia lining the lateral ventricles (Fig. 5). By SEM, the ependymal cilia are sparser, shorter and show a loss of dire ctional orientation that suggests they may be nonfunctional (Fig. 5A-F). By TEM, only 7% of $Jhy^{lacZ/lacZ}$ cilia show the normal 9+2 microtubule organization of motile cilia, with most having instead a 9+0 or 8+2 configuration (Fig. 5G-J, Fig. 8D). Normal nonmotile cilia display a 9+0 confirmation, indicating that the $Jhy^{lacZ/lacZ}$ 9+0 cilia are almost certainly immotile, but little is known about the potential motility of 8+2 cilia. The unique central pair morphology of 9+2 cilia is believed necessary for ciliary motility, with the central pair controlling the direction of the stroke. The abnormal doublet morphology of the central microtubules in the $Jhy^{lacZ/lacZ}$ 8+2 cilia suggest these cilia may also be immotile. Loss of ciliary motility leading to a failure to maintain CSF flow is therefore the predicted mechanism underling the $Jhy^{lacZ/lacZ}$ hydrocephalus. The JHY protein is not found in the ciliary proteome database (www.ciliome.com), but a recent bioinformatic-based study identified the predicted protein of the human homolog of Jhy ($C11ORF63$) in the cilia of adult human lung and oviduct (Ivliev et al., 2012).

Studies involving mouse models of hydrocephalus show a requirement for proper cilia structure and function in regulating CSF flow. Only two existing hydrocephalic models, however, show disruption of ciliary microtubule patterning. $Hsf1$ ($Heat shock transcription factor 1$)-null mice display reduced ciliary beat amplitude and frequency, and develop chronic sinusitis and communicating hydrocephalus (Takaki et al., 2007). Ultrastructural studies of $Hsf1$ respiratory epithelium showed that approximately 10% of cilia were structurally abnormal, with deletion and/or disorganization of the central pair and outer doublet microtubules. The abnormal cilia development in $Hsf1$ mutants was predicted to result from a secondary decrease in $Hsp90$ ($Heat shock protein 90$), which facilitates tubulin stability and polymerization (Takaki et al., 2007). Mice mutant for the $Stumpy$ gene develop hydrocephalus and polycystic kidney disease (Town et al., 2008). The ependymal cells of $Stumpy$ mutant animals contain intact basal bodies, but lack ciliary axonemes entirely. Localiz ation of STUMPY protein within the axonemes suggests it may be involved in the intraflagellar transport of proteins required for cilia outgrowth.

Regional gene expression is altered, and JHY protein is lost, in $Jhy^{lacZ/lacZ}$ mice

$Jhy^{lacZ/+}$ mice expressing 85% of the wild type level of Jhy do not develop hydrocephalus, while $Jhy^{lacZ/lacZ}$ mice expressing 41% of the wild type level develop hydrocephalus with a penetrance of 74%. These numbers suggest a threshold for Jhy expression, where the development of hydrocephalus occurs between 41-85% of wild type Jhy expression. The incomplete penetrance of the $Jhy^{lacZ/lacZ}$ hydrocephalus may therefore be due to stochastic events that subtly alter Jhy expression levels in $Jhy^{lacZ/lacZ}$ mice. In considering expression from the Jhy^{lacZ} allele, however, it is important to consider the transcripts that could be produced. The integration of a transcriptional termination codon suggests that Jhy^{lacZ} transcripts should contain at most the first 34% of the wild type transcript, which would encode 42% of the full length protein. Deletion of the first 88 bp of exon 5 dictate that any transcript produced beyond the integration site cannot be wild type in nature. The most likely mechanism for reconstructing a near-full length transcript, splicing from exon 4 to

exon 6, would generate an early stop codon. An antibody generated against the human JHY homolog C11ORF63 found JHY protein localized to the ventricular ependymal cells of $Jhy^{+/+}$ P5 mouse brains, while sections of $Jhy^{lacZ/lacZ}$ brains showed a significant reduction in JHY protein (Fig. 7). These data support a Jhy loss of function mechanism for the Jhy^{lacZ} mutation. Future studies will further characterize the protein products made from both $Jhy^{+/+}$ and Jhy^{lacZ} alleles.

Restoring a truncated version of the Jhy gene, roughly the same portion of the transcript as lies upstream of the Jhy^{lacZ} integration, provides significant rescue of the hydrocephalus phenotype (Fig. 8). $Tg^{BAC/+};Jhy^{lacZ/lacZ}$ animals show near-wild type levels of Jhy transcript when analyzed using primers span ning exon 2-3, and the phenotypic rescue suggests the mechanism is likely to be increased levels of a truncated protein. The JHY protein may therefore be modular in nature, where key domains within the remaining portion of the protein can provide partial function. There is some precedence for the rescue of ciliary defects, particularly structural defects, with gene fragments in other systems. A construct expressing just 35% of the $Chlamydomonas$ centriolar protein Bld10p gave partial rescue of the Bld10p deletion phenotype (Hiraki et al., 2007). Bld10p is a component of the radial spokes of the centriolar cartwheel, and the truncated protein allowed the assembly of largely normal flagella, but with shorter spokes and 8 rather than the expected 9 microtubule triplets.

Expression analysis showed decreased levels of Bsx in $Jhy^{lacZ/lacZ}$ brains, and no change in the expression of $Crtam$. Interestingly, the Bsx expression pattern overlaps with that predicted for Jhy in pineal gland and hypothalamus, though not in choroid plexus or ependyma (McArthur and Ohtoshi, 2007). There is no demonstrated role for Bsx in CSF balance or the development of hydrocephalus, and mouse models carrying a deletion of the Bsx gene are fully viable but display altered feeding and nursing behaviors (McArthur and Ohtoshi, 2007; Sakkou et al., 2007). $Crtam$ levels are not altered in $Jhy^{lacZ/lacZ}$ mice, and deletion of this gene displays no neural phenotype (Yeh et al., 2008). Taken together, these expression and rescue data provide strong support for altered function of the Jhy gene as causative for the $Jhy^{lacZ/lacZ}$ hydrocephalus. It remains formally possible that altered expression of Bsx may contribute in part to the $Jhy^{lacZ/lacZ}$ phenotype, and its absence from Tg^{BAC} may underlie the lack of full rescue. Ongoing experiments will generate a targeted deletion of the Jhy gene, along with additional Tg^{BAC} animals, to more clearly define all contributory factors.

Ependymal- and choroid plexus-based models for Jhy^{lacZ} hydrocephalus

At least two models can be proposed for the mechanism of the Jhy^{lacZ} hydrocephalus. First, loss of ciliary-mediated CSF flow may cause fluid accumulation in the ventricles resulting in hydrocephalus. Jhy appears to func tion in the ventricular ependymal cells to regulate cilia development, with loss of Jhy causing abnormally patterned ciliary microtubules. Hydrocephalus in the Jhy^{lacZ} mice arises as early as P1.5, suggesting the initiating event must precede this age. Previous analysis has shown that the ependymal cilia of the lateral ventricles develop between birth and P10, while the cilia lining the aqueduct of Sylvius are already present by P1 (Banizs et al., 2005; Spassky et al., 2005; Tissir et al., 2010). Our experiments find abundant cilia in the caudal region of the $Jhy^{+/+}$ lateral ventricles by P5, and these cilia are abnormal in $Jhy^{lacZ/lacZ}$ mice. JHY protein is present in the ependymal cells of the lateral ventricles at P5, and expression of the Jhy^{lacZ} reporter suggests expression in the ependymal cells lining the aqueduct at P0.5 (Fig. 4R, Fig. 7). These data are consistent with loss of ciliary function in the aqueductal and/or ventricular ependyma being causative for Jhy^{lacZ} hydrocephalus.

Expression from the *Jhy^{lacZ}* transgene is also found in the choroid plexus of the third ventricle, yet histological analysis of the choroid plexus by light microscopy shows no obvious abnormalities (Fig. 3D, Fig. 4L and data not shown). The choroid plexus epithelium carries motile cilia that develop by P1, though these cilia contribute minimally to bulk CSF flow and instead appear to function in a signaling pathway that regulates CSF production (Banizs et al., 2005). In the *Tg737^{orpk}* mutant mouse, loss of normal cilia function on the choroid plexus leads to excessive CSF production and hydrocephalus (Banizs et al., 2005). Abnormal choroid plexus cilia might therefore initiate hydrocephalus through CSF oversecretion, with loss of ventr icular ependymal flow exacerbating the increased fluid load. Further investigation of the choroid plexus cilia will determine their role in the development of hydrocephalus in *Jhy^{lacZ/lacZ}* mice.

Supplementary Material

Refer to Web version on PubMed Central for supplementary material.

Acknowledgments

REFERENCES

al-Shroof M, Karnik AM, Karnik AA, Longshore J, Sliman NA, Khan FA. Ciliary dyskinesia associated with hydrocephalus and mental retardation in a Jordanian family. Mayo Clinic Proceedings. 2001; 76:1219–1224. [PubMed: 11761503]

Allen ND, Cran DG, Barton SC, Hettle S, Reik W, Surani MA. Transgenes as probes for active chromosomal domains in mouse development. Nature. 1988; 333:852–855. [PubMed: 3386733]

Auffray C, Rougeon F. Purification of mouse immunoglobulin heavy-chain messenger RNAs from total myeloma tumor RNA. European Journal of Biochemistry. 1980; 107:303–314. [PubMed: 6772444]

Baker K, Beales PL. Making sense of cilia in disease: the human ciliopathies. American Journal of Medical Genetics. Part C, Seminars in Medical Genetics. 2009; 151C:281–295.

Banizs B, Pike MM, Millican CL, Ferguson WB, Komlosi P, Sheetz J, Bell PD, Schwiebert EM, Yoder BK. Dysfunctional cilia lead to altered ependyma and choroid plexus function, and result in the formation of hydrocephalus. Development. 2005; 132:5329–5339. [PubMed: 16284123]

Batiz LF, Paez P, Jimenez AJ, Rodriguez S, Wagner C, Perez-Figares JM, Rodriguez EM. Heterogeneous expression of hydrocephalic phenotype in the hyh mice carrying a point mutation in alpha-SNAP. Neurobiology of Disease. 2006; 23:152–168. [PubMed: 16697210]

Bhadelia RA, Bogdan AR, Kaplan RF, Wolpert SM. Cerebrospinal fluid pulsation amplitude and its quantitative relationship to cerebral blood flow pulsations: a phase-contrast MR flow imaging study. Neuroradiology. 1997; 39:258–264. [PubMed: 9144672]

Blackburn BL, Fineman RM. Epidemiology of congenital hydrocephalus in Utah, 1940-1979: report of an iatrogenically related "epidemic". American Journal of Medical Genetics. 1994; 52:123–129. [PubMed: 7801996]

Blackshear PJ, Graves JP, Stumpo DJ, Cobos I, Rubenstein JL, Zeldin DC. Graded phenotypic response to partial and complete deficiency of a brain-specific transcript variant of the winged helix transcription factor RFX4. Development. 2003; 130:4539–4552. [PubMed: 12925582]

Bradley JP, Levine JP, Roth DA, McCarthy JG, Longaker MT. Studies in cranial suture biology: IV. Temporal sequence of posterior frontal cranial suture fusion in the mouse. Plastic and Reconstructive Surgery. 1996; 98:1039–1045. [PubMed: 8911474]

Bruni JE. Ependymal development, proliferation, and functions: a review. Microscopy Research and Technique. 1998; 41:2–13. [PubMed: 9550133]

Castro-Gago M, Alonso A, Eiris-Punal J. Autosomal recessive hydrocephalus with aqueductal stenosis. Child's Nervous System. 1996; 12:188–191.

Chalmers RM, Andreae L, Wood NW, Durai Raj RV, Casey AT. Familial hydrocephalus. Journal of Neurology, Neurosurgery & Psychiatry. 1999; 67:410–411.

Chow CW, McKelvie PA, Anderson RM, Phelan EM, Klug GL, Rogers JG. Autosomal recessive hydrocephalus with third ventricle obstruction. American Journal of Medical Genetics. 1990; 35:310–313. [PubMed: 2178419]

Christensen JH, Hansen LK, Garne E. [Congenital hydrocephalus--prevalence and prognosis. Mortality and morbidity in a population-based study]. Ugeskr Laeger. 2003; 165:466–469. [PubMed: 12599846]

Chudley AE, McCullough C, McCullough DW. Bilateral sensorineural deafness and hydrocephalus due to foramen of Monro obstruction in sibs: a newly described autosomal recessive disorder. American Journal of Medical Genetics. 1997; 68:350–356. [PubMed: 9024571]

Davson, H.; Segal, MB. Physiology of the CSF and blood-brain barriers. CRC Press; Boca Raton, FL: 1996.

Davy BE, Robinson ML. Congenital hydrocephalus in hy3 mice is caused by a frameshift mutation in Hydin, a large novel gene. Human Molecular Genetics. 2003; 12:1163–1170. [PubMed: 12719380]

Fay TN, Jacobs I, Teisner B, Poulsen O, Chapman MG, Stabile I, Bohn H, Westergaard JG, Grudzinskas JG. Two fetal antigens (FA-1 and FA-2) and endometrial proteins (PP12 and PP14) isolated from amniotic fluid; preliminary observations in fetal and maternal tissues. European Journal of Obstetrics, Gynecology, and Reproductive Biology. 1988; 29:73–85.

Feng X, Papadopoulos MC, Liu J, Li L, Zhang D, Zhang H, Verkman AS, Ma T. Sporadic obstructive hydrocephalus in Aqp4 null mice. Journal of Neuroscience Research. 2009; 87:1150–1155. [PubMed: 18951529]

Ferkol TW, Leigh MW. Ciliopathies: the central role of cilia in a spectrum of pediatric disorders. Journal of Pediatrics. 2012; 160:366–371. [PubMed: 22177992]

Gadsdon DR, Variend S, Emery JL. Myelination of the corpus callosum. II. The effect of relief of hydrocephalus upon the processes of myelination. Z Kinderchir Grenzgeb. 1979; 28:314–321. [PubMed: 551615]

Green MC. The developmental effects of congenital hydrocephalus (ch) in the mouse. Developmental Biology. 1970; 23:585–608. [PubMed: 5500588]

Greitz D. Cerebrospinal fluid circulation and associated intracranial dynamics. A radiologic investigation using MR imaging and radionuclide cisternography. Acta Radiologica Supplement. 1993; 386:1–23.

Hamada H, Watanabe H, Sugimoto M, Yasuoka M, Yamada N, Kubo T. Autosomal recessive hydrocephalus due to congenital stenosis of the aqueduct of Sylvius. Prenatal Diagnosis. 1999; 19:1067–1069. [PubMed: 10589063]

Haverkamp F, Wolfle J, Aretz M, Kramer A, Hohmann B, Fahnenstich H, Zerres K. Congenital hydrocephalus internus and aqueduct stenosis: aetiology and implications for genetic counselling. European Journal of Pediatrics. 1999; 158:474–478. [PubMed: 10378395]

Hiraki M, Nakazawa Y, Kamiya R, Hirono M. Bld10p constitutes the cartwheel-spoke tip and stabilizes the 9-fold symmetry of the centriole. Current Biology. 2007; 17:1778–1783. [PubMed: 17900905]

Ibanez-Tallon I, Pagenstecher A, Fliegauf M, Olbrich H, Kispert A, Ketelsen UP, North A, Heintz N, Omran H. Dysfunction of axonemal dynein heavy chain Mdnah5 inhibits ependymal flow and reveals a novel mechanism for hydrocephalus formation. Human Molecular Genetics. 2004; 13:2133–2141. [PubMed: 15269178]

Ivliev AE, t Hoen PA, van Roon-Mom WM, Peters DJ, Sergeeva MG. Exploring the transcriptome of ciliated cells using in silico dissection of human tissues. PloS One. 2012; 7:e35618. [PubMed: 22558177]

Jones HC, Bucknall RM. Inherited prenatal hydrocephalus in the H-Tx rat: a morphological study. Neuropathology and Applied Neurobiology. 1988; 14:263–274. [PubMed: 3221976]

Koh L, Zakharov A, Nagra G, Armstrong D, Friendship R, Johnston M. Development of cerebrospinal fluid absorption sites in the pig and rat: connections between the subarachnoid space and lymphatic vessels in the olfactory turbinates. Anatomy & Embryology. 2006; 211:335–344. [PubMed: 16528517]

Koh S, Boles RG. Cerebral aqueductal stenosis as a presentation of deletion 6q25-qter. Clinical Genetics. 1998; 53:317–318. [PubMed: 9650774]

Krebs DL, Metcalf D, Merson TD, Voss AK, Thomas T, Zhang JG, Rakar S, O'Bryan MK, Willson TA, Viney EM, Mielke LA, Nicola NA, Hilton DJ, Alexander WS. Development of hydrocephalus in mice lacking SOCS7. Proceedings of the National Academy of Sciences. 2004; 101:15446–15451.

Kume T, Deng KY, Winfrey V, Gould DB, Walter MA, Hogan BL. The forkhead/winged helix gene Mf1 is disrupted in the pleiotropic mouse mutation congenital hydrocephalus. Cell. 1998; 93:985–996. [PubMed: 9635428]

Laborda J, Sausville EA, Hoffman T, Notario V. dlk, a putative mammalian homeotic gene differentially expressed in small cell lung carcinoma and neuroendocrine tumor cell line. Journal of Biological Chemistry. 1993; 268:3817–3820. [PubMed: 8095043]

Lechtreck KF, Delmotte P, Robinson ML, Sanderson MJ, Witman GB. Mutations in Hydin impair ciliary motility in mice. Journal of Cell Biology. 2008; 180:633–643. [PubMed: 18250199]

Lee L. Mechanisms of mammalian ciliary motility: Insights from primary ciliary dyskinesia genetics. Gene. 2011; 473:57–66. [PubMed: 21111794]

Lindeman GJ, Dagnino L, Gaubatz S, Xu Y, Bronson RT, Warren HB, Livingston DM. A specific, nonproliferative role for E2F-5in choroid plexus function revealed by gene targeting. Genes & Development. 1998; 12:1092–1098. [PubMed: 9553039]

McArthur T, Ohtoshi A. A brain-specific homeobox gene, Bsx, is essential for proper postnatal growth and nursing. Molecular & Cellular Biology. 2007; 27:5120–5127. [PubMed: 17485440]

Munch TN, Rostgaard K, Rasmussen ML, Wohlfahrt J, Juhler M, Melbye M. Familial aggregation of congenital hydrocephalus in a nationwide cohort. Brain. 2012; 135:2409–2415. [PubMed: 22763745]

Oi S, Di Rocco C. Proposal of "evolution theory in cerebrospinal fluid dynamics" and minor pathway hydrocephalus in developing immature brain. Childs Nervous System. 2006; 22:662–669.

Okamoto M, Takemori H, Halder SK, Hatano O. Zona glomerulosa-specific factor: cloning and function. Steroids. 1997; 62:73–76. [PubMed: 9029718]

Osoegawa K, Tateno M, Woon PY, Frengen E, Mammoser AG, Catanese JJ, Hayashizaki Y, de Jong PJ. Bacterial artificial chromosome libraries for mouse sequencing and functional analysis. Genome Research. 2000; 10:116–128. [PubMed: 10645956]

Partington MD. Congenital hydrocephalus. Neurosurgery Clinics of North America. 2001; 12:737–742. ix. [PubMed: 11524294]

Pattisapu JV. Etiology and clinical course of hydrocephalus. Neurosurgery Clinics of North America. 2001; 12:651–659. vii. [PubMed: 11524287]

Portenoy RK, Berger A, Gross E. Familial occurrence of idiopathic normal-pressure hydrocephalus. Archives of Neurology. 1984; 41:335–337. [PubMed: 6696655]

Quencer RM, Post MJ, Hinks RS. Cine MR in the evaluation of normal and abnormal CSF flow: intracranial and intraspinal studies. Neuroradiology. 1990; 32:371–391. [PubMed: 2259432]

Rodriguez EM. The cerebrospinal fluid as a pathway in neuroendocrine integration. Journal of Endocrinology. 1976; 71:407–443. [PubMed: 794431]

Rogers ED, Ramalie JR, McMurray EN, Schmidt JV. Localizing transcriptional regulatory elements at the mouse Dlk1 locus. PloS One. 2012; 7:e36483. [PubMed: 22606264]

Rosenthal A, Jouet M, Kenwrick S. Aberrant splicing of neural cell adhesion molecule L1 mRNA in a family with X-linked hydrocephalus. Nature Genetics. 1992; 2:107–112. [PubMed: 1303258]

Rudas G, Almassy Z, Papp B, Varga E, Meder U, Taylor GA. Echodense spinal subarachnoid space in neonates with progressive ventricular dilatation: a marker of noncommunicating hydrocephalus. American Journal of Roentgenology. 1998; 171:1119–1121. [PubMed: 9763007]

Sakkou M, Wiedmer P, Anlag K, Hamm A, Seuntjens E, Ettwiller L, Tschop MH, Treier M. A role for brain-specific homeobox factor Bsx in the control of hyperphagia and locomotory behavior. Cell Metabolism. 2007; 5:450–463. [PubMed: 17550780]

Sapiro R, Kostetskii I, Olds-Clarke P, Gerton GL, Radice GL, Strauss J. Male infertility, impaired sperm motility, and hydrocephalus in mice deficient in sperm-associated antigen 6. Molecular & Cellular Biology. 2002; 22:6298–6305. [PubMed: 12167721]

Schrander-Stumpel C, Fryns JP. Congenital hydrocephalus: nosology and guidelines for clinical approach and genetic counselling. European Journal of Pediatrics. 1998; 157:355–362. [PubMed: 9625330]

Smas CM, Sul HS. Pref-1, a protein containing EGF-like repeats, inhibits adipocyte differentiation. Cell. 1993; 73:725–734. [PubMed: 8500166]

Spassky N, Merkle FT, Flames N, Tramontin AD, Garcia-Verdugo JM, Alvarez-Buylla A. Adult ependymal cells are postmitotic and are derived from radial glial cells during embryogenesis. Journal of Neuroscience. 2005; 25:10–18. [PubMed: 15634762]

Stoll C, Alembik Y, Dott B, Roth MP. An epidemiologic study of environmental and genetic factors in congenital hydrocephalus. European Journal of Epidemiology. 1992; 8:797–803. [PubMed: 1294384]

Takaki E, Fujimoto M, Nakahari T, Yonemura S, Miyata Y, Hayashida N, Yamamoto K, Vallee RB, Mikuriya T, Sugahara K, Yamashita H, Inouye S, Nakai A. Heat shock transcription factor 1 is required for maintenance of ciliary beating in mice. Journal of Biological Chemistry. 2007; 282:37285–37292. [PubMed: 17965413]

Tissir F, Qu Y, Montcouquiol M, Zhou L, Komatsu K, Shi D, Fujimori T, Labeau J, Tyteca D, Courtoy P, Poumay Y, Uemura T, Goffinet AM. Lack of cadherins Celsr2 and Celsr3 impairs ependymal ciliogenesis, leading to fatal hydrocephalus. Nature Neuroscience. 2010; 13:700–707.

Town T, Breunig JJ, Sarkisian MR, Spilianakis C, Ayoub AE, Liu X, Ferrandino AF, Gallagher AR, Li MO, Rakic P, Flavell RA. The stumpy gene is required for mammalian ciliogenesis. Proceedings of the National Academy of Sciences. 2008; 105:2853–2858.

Tullio AN, Bridgman PC, Tresser NJ, Chan CC, Conti MA, Adelstein RS, Hara Y. Structural abnormalities develop in the brain after ablation of the gene encoding nonmuscle myosin II-B heavy chain. Journal of Comparative Neurology. 2001; 433:62–74. [PubMed: 11283949]

Uhlen M, Oksvold P, Fagerberg L, Lundberg E, Jonasson K, Forsberg M, Zwahlen M, Kampf C, Wester K, Hober S, Wernerus H, Bjorling L, Ponten F. Towards a knowledge-based Human Protein Atlas. Nature Biotechnology. 2010; 28:1248–1250.

Verhagen WI, Bartels RH, Fransen E, van Camp G, Renier WO, Grotenhuis JA. Familial congenital hydrocephalus and aqueduct stenosis with probably autosomal dominant inheritance and variable expression. Journal of the Neurological Sciences. 1998; 158:101–105. [PubMed: 9667786]

Vincent C, Kalatzis V, Compain S, Levilliers J, Slim R, Graia F, Pereira ML, Nivelon A, Croquette MF, Lacombe D, et al. A proposed new contiguous gene syndrome on 8q consists of Branchio-Oto-Renal (BOR) syndrome, Duane syndrome, a dominant form of hydrocephalus and trapeze aplasia; implications for the mapping of the BOR gene. Human Molecular Genetics. 1994; 3:1859–1866. [PubMed: 7849713]

Welch K. Secretion of cerebrospinal fluid by choroid plexus of the rabbit. American Journal of Physiology. 1963; 205:617–624. [PubMed: 14065919]

Weller RO, Kida S, Zhang ET. Pathways of fluid drainage from the brain--morphological aspects and immunological significance in rat and man. Brain Pathology. 1992; 2:277–284. [PubMed: 1341963]

Wessels MW, den Hollander NS, Willems PJ. Mild fetal cerebral ventriculomegaly as a prenatal sonographic marker for Kartagener syndrome. Prenatal Diagnosis. 2003; 23:239–242. [PubMed: 12627427]

Wilson GR, Wang HX, Egan GF, Robinson PJ, Delatycki MB, O'Bryan MK, Lockhart PJ. Deletion of the Parkin co-regulated gene causes defects in ependymal ciliary motility and hydrocephalus in the quakingviable mutant mouse. Human Molecular Genetics. 2010; 19:1593–1602. [PubMed: 20106870]

Wood, J. Physiology, pharmacology and dynamics of cerebrospinal fluid. Plenum Press; New York: 1983.

Worthington WC, Cathcart RS. Ciliary currents on ependymal surfaces. Annals of the New York Academy of Sciences. 1966; 130:944–950. [PubMed: 5222720]

Yamadori T, Nara K. The directions of ciliary beat on the wall of the lateral ventricle and the currents of the cerebrospinal fluid in the brain ventricles. Scanning Electron Microscopy. 1979:335–340. [PubMed: 524006]

Yeh JH, Sidhu SS, Chan AC. Regulation of a late phase of T cell polarity and effector functions by Crtam. Cell. 2008; 132:846–859. [PubMed: 18329370]

Yevtodiyenko A, Steshina EY, Farner SC, Levorse JM, Schmidt JV. A 178-kb BAC transgene imprints the mouse Gtl2 gene and localizes tissue-specific regulatory elements. Genomics. 2004; 84:277–287. [PubMed: 15233992]

HIGHLIGHTS

Jhy^{lacZ} transgenic mice develop autosomal recessive communicating hydrocephalus.

The *Jhy* gene produces a conserved protein with no known functional domains.

Ependymal cilia in *Jhy^{lacZ}* brains are disorganized and randomly oriented.

*Jhy^{lacZ}* cilia have abnormal 9+0 and 8+2 microtubule organization patterns.
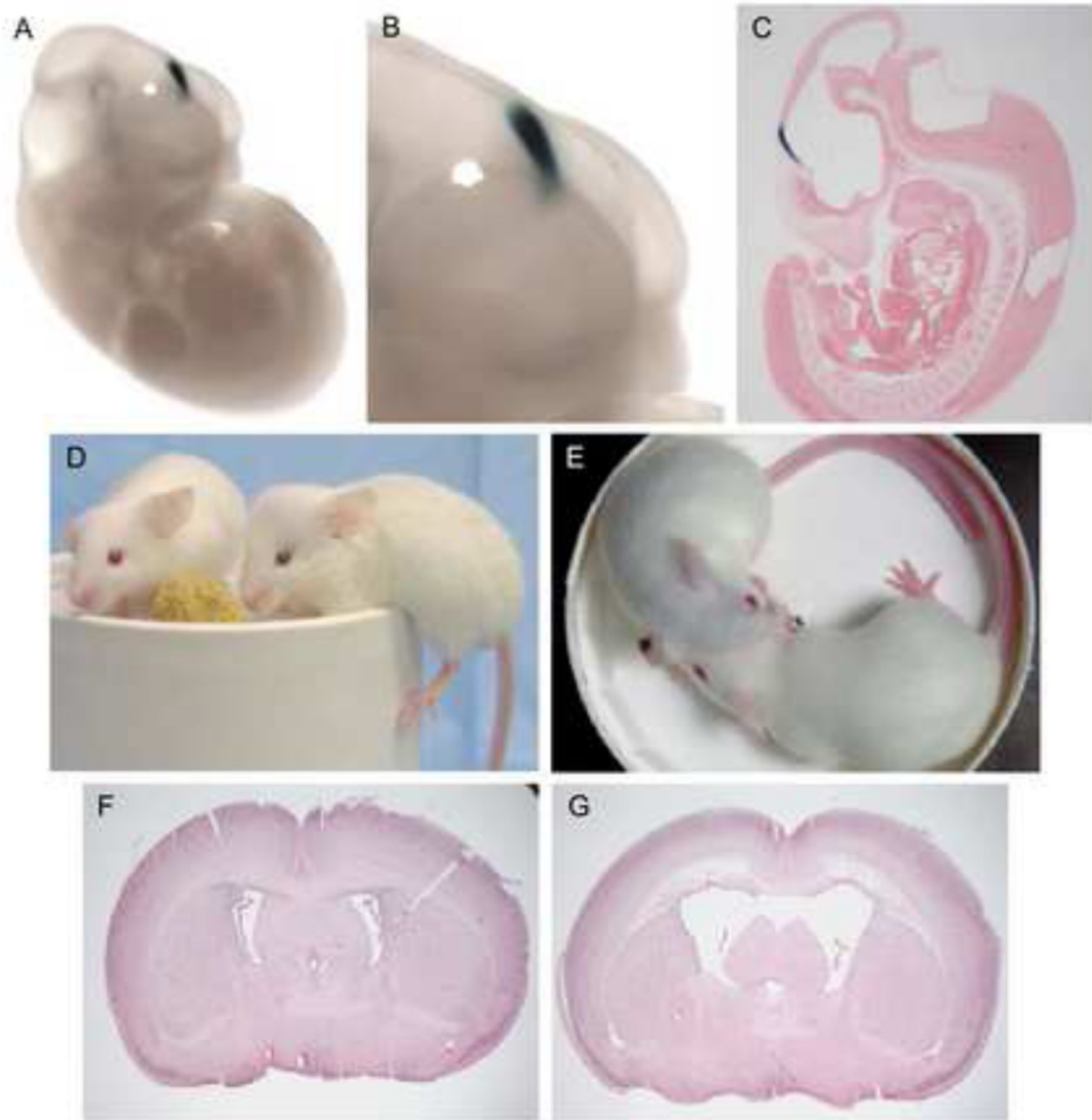
Figure 1. $Jhy^{lacZ/lacZ}$ mice develop hydrocephalus
A) $Jhy^{lacZ/lacZ}$ embryo at e11.5 showing *lacZ* expression in the epi physis of the diencephalon. B) Enlarged view of *lacZ* expression in A. C) Saggital section of diencephalon *lacZ* expression in e11.5 $Jhy^{lacZ/lacZ}$ embryo. D) $Jhy^{+/+}$ (left) and $Jhy^{lacZ/lacZ}$ littermates (right) at 3 weeks of age, showing doming of the skull and ataxia in the $Jhy^{lacZ/lacZ}$ mouse. E) Hemorrhaging beneath the skull is visible in a 3 week old $Jhy^{lacZ/lacZ}$ mouse (top) compared to a $Jhy^{+/+}$ littermate (bottom). F, G) Hematoxylin/eosin stained sections of $Jhy^{+/+}$ (F) and $Jhy^{lacZ/lacZ}$ (G) brains at P5, showing ventricular dilation.
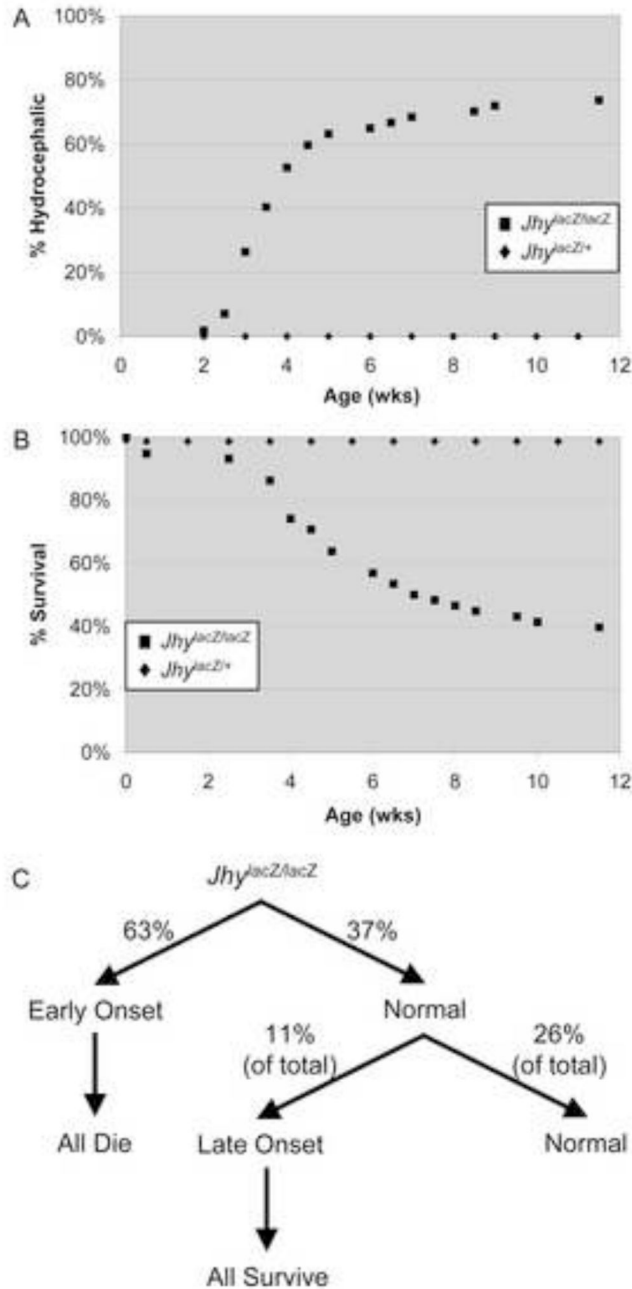
Figure 2. $Jhy^{lacZ/lacZ}$ hydrocephalus is rapid and progressive
A) $Jhy^{lacZ/lacZ}$ mice (squares) develop outwardly visible hydrocephalus with a penetrance of 74%, with most mice affected by 5 weeks of age. No $Jhy^{lacZ/+}$ mice (diamonds) developed hydrocephalus or died during the 12 week monitoring period. B) Most $Jhy^{lacZ/lacZ}$ mice die by 4-8 weeks of age. C) Early onset hydrocephalus occurs in 63% of $Jhy^{lacZ/lacZ}$ mice, with an additional 11% developing a late onset milder form of the disease.
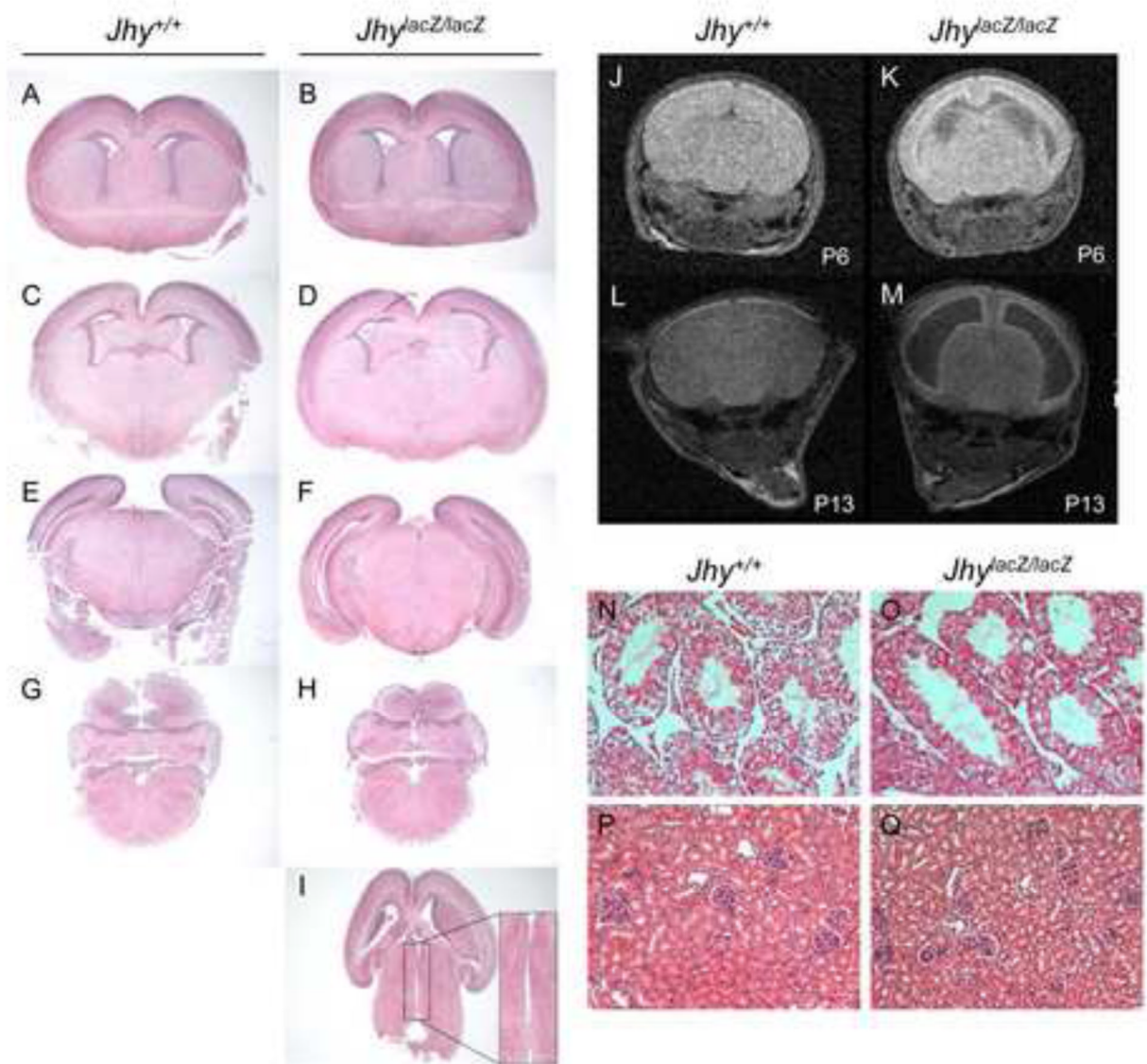
Figure 3. *Jhy^lacZ/lacZ* brains show normal development and patterning
A-H) Coronal sections of *Jhy^+/+* and *Jhy^lacZ/lacZ* brains at P0.5 show normal morphology and patterning. I) Transverse section of *Jhy^lacZ/lacZ* brain at P0.5 shows a patent aqueduct. The inset shows an enlarged image of the aqueduct. J-M) Magnetic resonance imaging of *Jhy^+/+* and *Jhy^lacZ/lacZ* brains. J, K) MRI at P6 shows significant dilation of the lateral ventricles of the *Jhy^lacZ/lacZ* mouse (K) as compared to a *Jhy^+/+* littermate (J). L, M) MRI at P13 shows more pronounced ventricular dilation with loss of brain tissue. N-Q) Adult testis (N, O) shows reduced numbers of mature sperm, while kidney (P, Q) shows normal development.
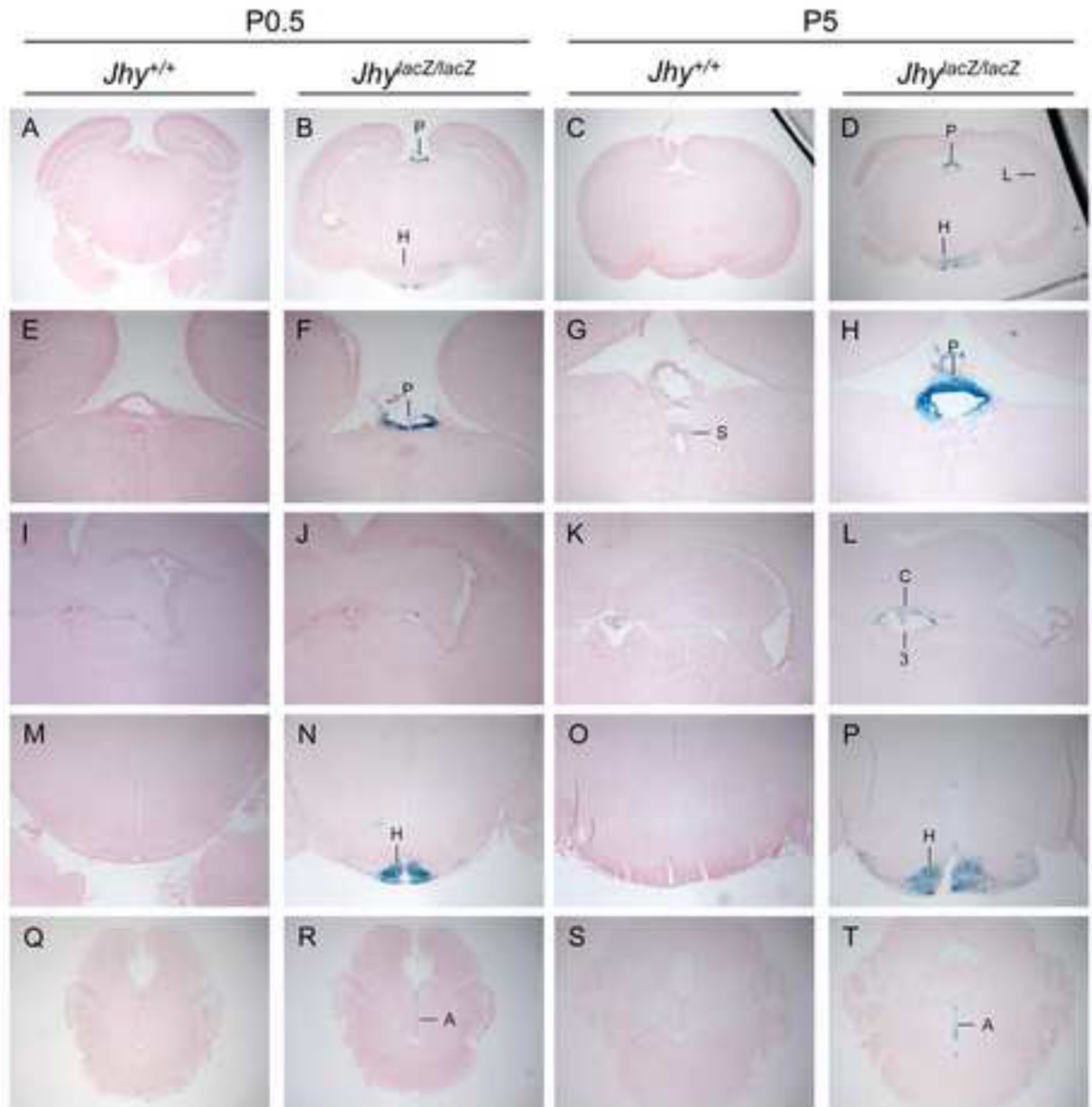
Figure 4. Jhy^{lacZ} transge ne reporter expression in the brain

Jhy^{lacZ} transgene expression was examined in $Jhy^{+/+}$ and $Jhy^{lacZ/lacZ}$ mice at P0.5 and P5. A-D) Expression of the *lacZ* reporter is observed in the pineal gland and hypothalamus at P0.5 and P5. Dilation of the lateral ventricles can be seen in $Jhy^{lacZ/lacZ}$ mice at P5. E-H) Higher magnification of the pineal gland *lacZ* expression, and lack of expression in the subcommissural organ. I-L) Expression of *lacZ* is seen in the choroid plexus of the third ventricle at P5, but not in the choroid plexus or ependyma of the lateral ventricles. At P5 dilation of the third ventricle is seen in $Jhy^{lacZ/lacZ}$ mice. M-P) Higher magnification of the hypothalamus *lacZ* expression. Q-T) Expression of *lacZ* in the ependyma lining the aqueduct of Sylvius. Structures are indicated as follows: A, aqueduct of Sylvius; C, choroid

plexus; H, hypothalamus; L, lateral ventricle; P, pineal gland; S, subcommissural organ; 3, third ventricle.
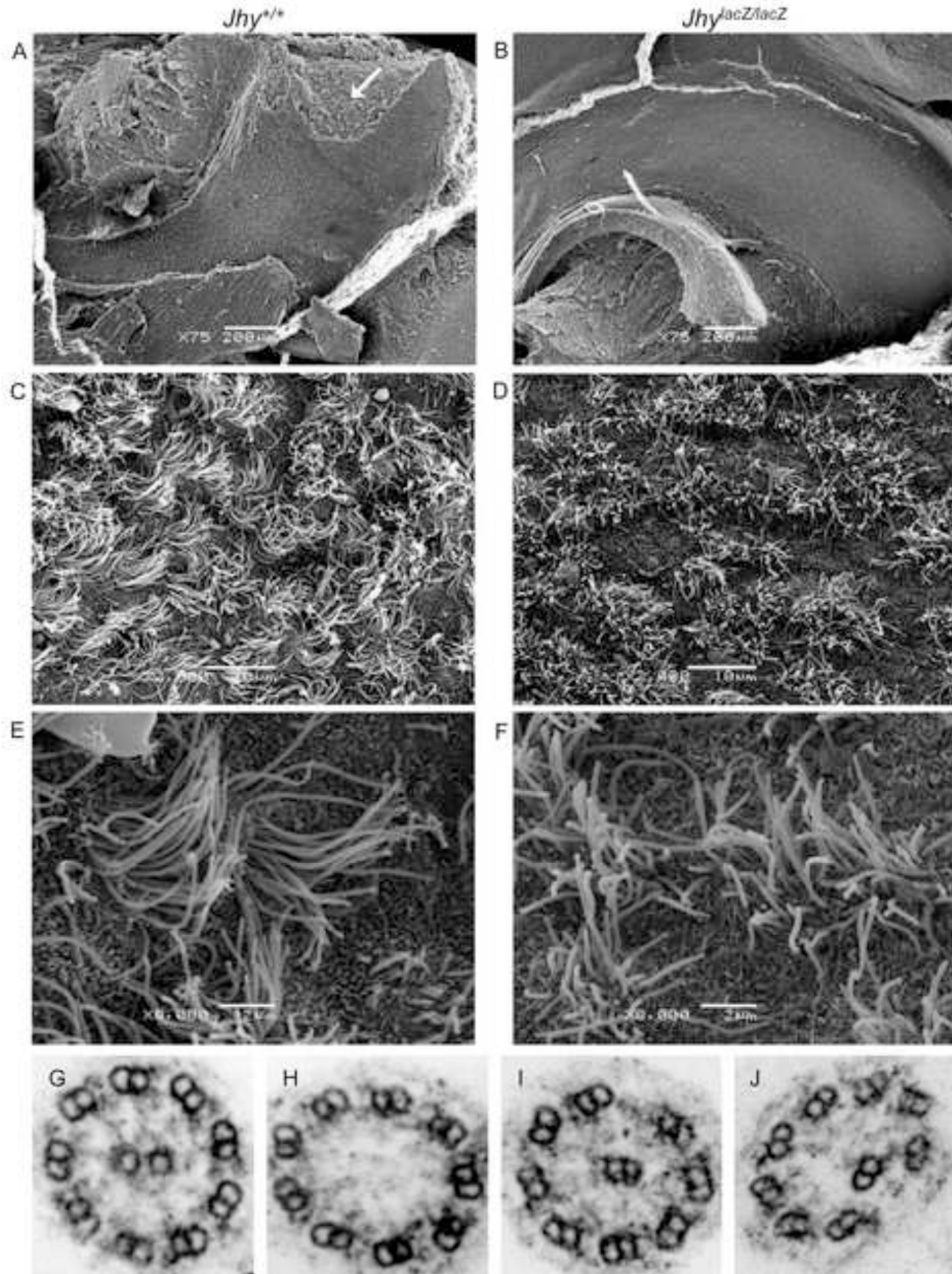
Figure 5. $Jhy^{lacZ/lacZ}$ ependymal cilia exhibit structural abnormalities
A-B) SEM was used to visualize the ultrastructure of the ependymal cilia in P5 $Jhy^{+/+}$ (A)
and $Jhy^{lacZ/lacZ}$ (B) lateral ventricles. Caudal is to the left. C-D) Higher magnification
images of the ependymal cilia in P5 $Jhy^{+/+}$ (C) and $Jhy^{lacZ/lacZ}$ (D) lateral ventricles. E-F)
High magnification images of the ependymal cilia in P5 $Jhy^{+/+}$ (E) and $Jhy^{lacZ/lacZ}$ (F)
lateral ventricles. G-I) Representative TEM images of $Jhy^{+/+}$ 9+2 (G), and $Jhy^{lacZ/lacZ}$ 9+0
(H) and 8+2 (I) axonemes. J) TEM image showing partial displacement of a peripheral ring
microtubule doublet towards the center of the axoneme in a $Jhy^{lacZ/lacZ}$ brain. Magnification
for all TEM images is 100,000X. Corresponding regions of the lateral ventricle were

examined in each mouse (n = 3 each for *Jhy*$^{+/+}$ and *Jhy*$^{lacZ/lacZ}$), and representative images were taken with scale bars embedded at 75× (A, B), 2,000× (C, D), and 8,000× (E, F).
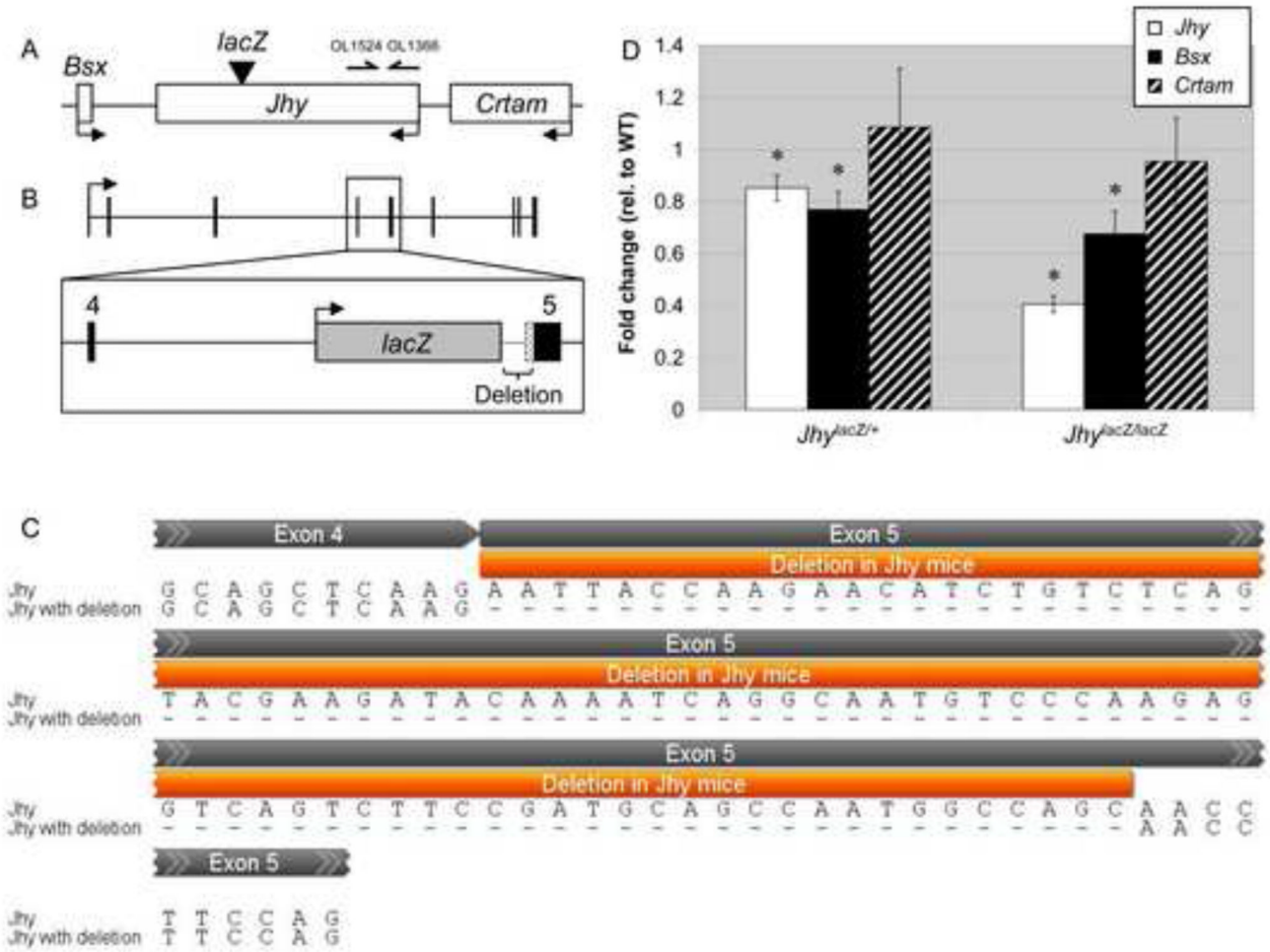
Figure 6. The *Jhy^lacZ* transgene disrupts the uncharacterized gene *4931429I11Rik* (*Jhy*)
A) The *Jhy^lacZ* transgene integrated within the *Jhy* gene on mouse chromosome 9. Boxes denote the *Jhy* gene and flanking genes *Bsx* and *Crtam*, the arrowhead indicates the *Jhy^lacZ* integration, the arrows indicate the direction of transcription and the primers used for qRT-PCR are denoted with half-arrows. B) The *Jhy^lacZ* transgene integrated at the beginning of *Jhy* exon 5, generating a deletion that removes 425 bp of intron 4 and the first 88 bp of exon 5. The black boxes represent *Jhy* exons, the grey box the *Jhy^lacZ* transgene, the dotted line the intronic sequence deleted, and the bracket indicates the entire deletion. (In this view the chromosomal orientation of the *Jhy* gene has been rotated for clarity.) C) *Jhy* exons 4 and 5 are juxtaposed to show the exon 5 sequence deleted. D) qRT-PCR analysis of the expression levels of *Jhy* (white bars), *Bsx* (black bars), and *Crtam* (hatched bars) in P0.5 *Jhy^lacZ/+* and *Jhy^lacZ/lacZ* brain in comparison to *Jhy^+/+* levels (n   7 for all genotypes), * denotes p   0.05.
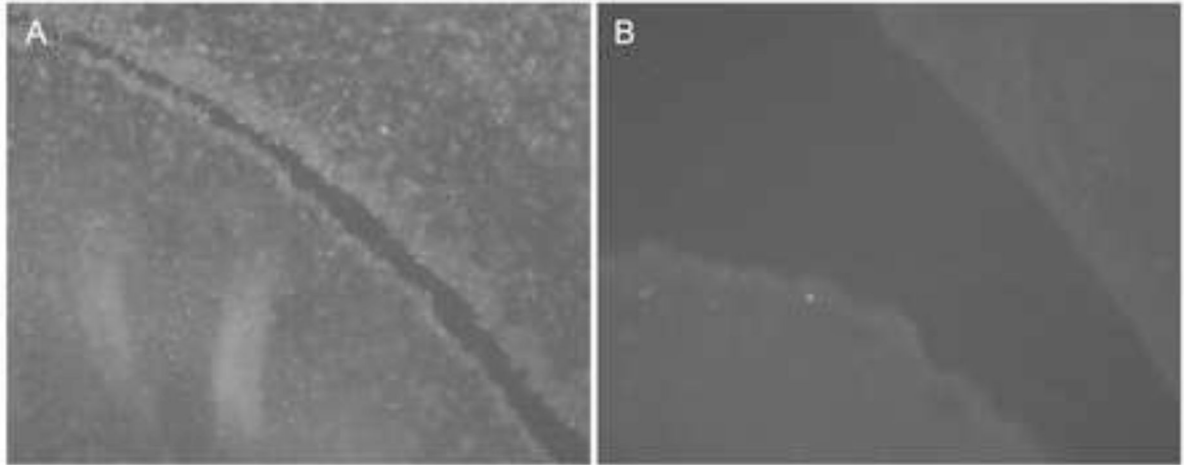
Figure 7. *Jhy^lacZ/lacZ* mice express reduced levels of JHY protein
A) JHY protein localizes to the ependymal cells of the lateral ventricle in *Jhy^+/+* P5 mouse brain using an antibody directed against the human JHY homolog C11ORF63. B) *Jhy^lacZ/lacZ* brain shows significantly reduced levels of JHY protein.
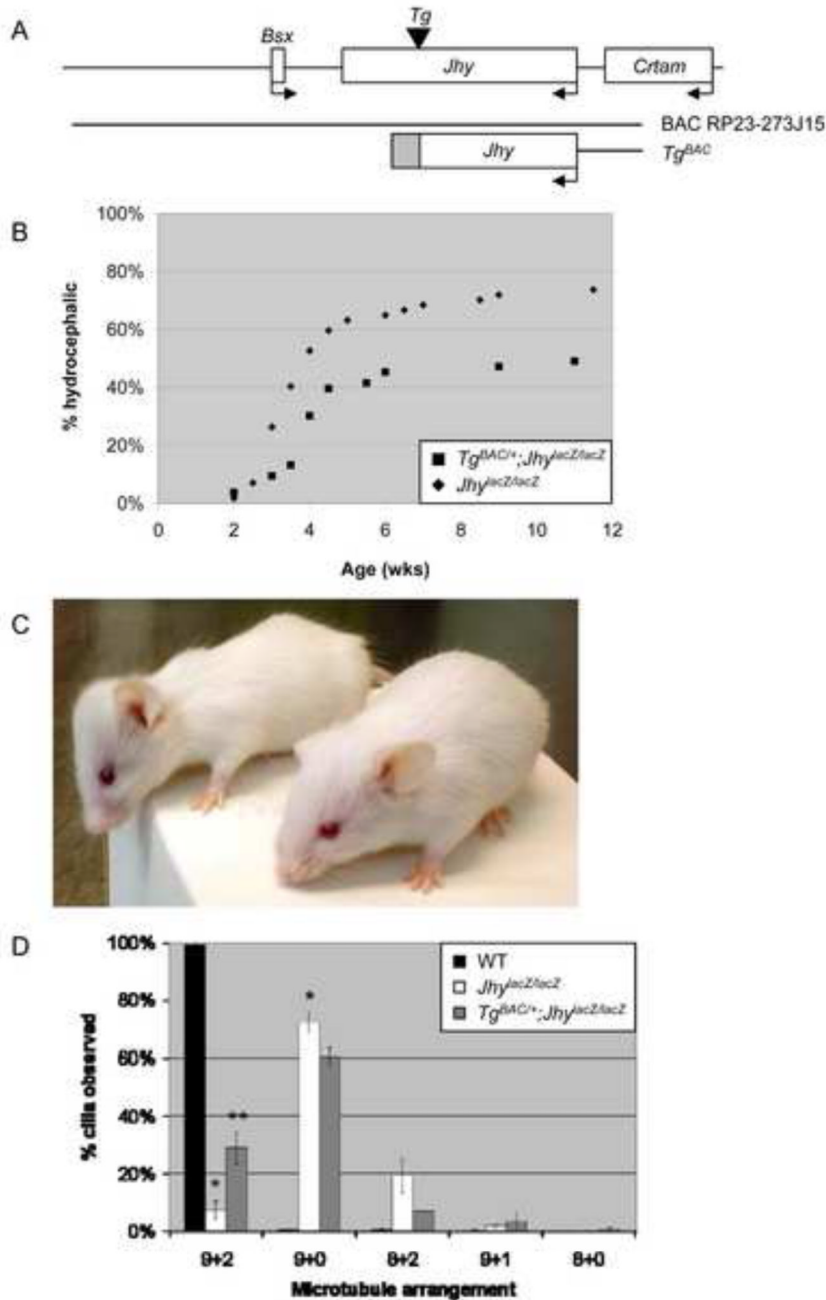
Figure 8. Transgenic rescue of *Jhy^{lacZ/lacZ}* mice
A) The RP23-273J15 BAC clone spans the region 80 kb proximal to 20 kb distal to the *Jhy* gene, while the integrated *Tg^{BAC}* has been truncated to contain 60-70% of the protein coding region of *Jhy*. The white boxes represent the *Bsx, Jhy* and *Crtam* genes, the arrowhead indicates the *Jhy^{lacZ}* integration, the arrows indicate the direction of gene transcription, the grey box indicates the end of the truncated portion of *Tg^{BAC}* that cannot be defined due to a lack of SNPs. B) The incidence of hydrocephalus is reduced from 74% in *Jhy^{lacZ/lacZ}* mice (diamonds) to 37% in *Tg^{BAC/+}*;*Jhy^{lacZ/lacZ}* mice (squares). C) Image of *Jhy^{lacZ/lacZ}* (left) and *Tg^{BAC/+}*;*Jhy^{lacZ/lacZ}* (right) littermates showing phenotypic rescue by *Tg^{BAC}*. D) Quantification of TEM analysis of ependymal ciliary microtubule arrangement in

$Jhy^{+/+}$ (black bars), $Jhy^{lacZ/lacZ}$ (white bars) and $Tg^{BAC/+}$;$Jhy^{lacZ/lacZ}$ (grey bars) at P5 (n=620 for $Jhy^{+/+}$, 147 for $Jhy^{lacZ/lacZ}$, and 117 for $Tg^{BAC/+}$;$Jhy^{lacZ/lacZ}$), * denotes p   0.05 relative to $Jhy^{+/+}$, ** denotes p   0.05 relative to $Jhy^{lacZ/lacZ}$.